JOURNAL OF COMPUTATIONAL PYSICS 54, 325–362 (1984)

A Fully Multidimensional Positive Definite Advection Transport Algorithm with Small Implicit Diffusion

PIOTR K. SMOLARKIEWICZ*

National Center for Atmospheric Research,† Boulder, Colorado 80307

Received July 8, 1983

The idea of the simple positive definite advection scheme presented previously in *Monthly Weather Review* (**111** (1983), 479) is improved for an optional multidimensional case and is presented in a generalized format. The accuracy of the scheme is discussed and a review of existing options is presented and illustrated through numerical tests.

1. INTRODUCTION

In numerical modeling of physical phenomena it is often necessary to solve the advective transport equation for positive definite scalar functions. Numerical schemes of second- or higher-order accuracy can produce negative values in the solution due to the dispersive ripples. Lower-order schemes, such as the donor cell or Lax–Friedrichs, or higher-order schemes with zeroth-order diffusion added produce no ripples but suffer from excessive implicit diffusion. In the last ten years a possible resolution of this dilemma has been developed in the form of hybrid schemes, in which the advective fluxes are given as a weighted average of a first-order positive definite scheme's fluxes and a higher-order scheme's fluxes. The difference in determination of the weights in the calculation of the average advective fluxes has led to different hybrid schemes. Two main hybrid-type schemes have been developed. One, the so called flux-corrected transport (FCT) method, was originated by Boris and Book [1–3] and generalized by Zalesak [14]; the other was developed by Harten and Zwas [6, 9] in the form of the self-adjusting hybrid schemes (SAHS) method. Both methods were constructed to deal effectively with shocks and contact discontinuities. Solutions of the advection transport equation obtained by using FCT or SAHS maintain positive definiteness of the initial condition and, as can be seen from presented tests (Zalesak [14], Harten [6]), be very accurate. Unfortunately, application of these methods to the modeling of complex multidimensional hydrodynamical systems like atmospheric phenomena is rather limited due to the excessive computer time required. Furthermore, in many hydrodynamical systems,

* On leave from the Institute of Geophysics, Warsaw University, Poland.

† The National Center for Atmospheric Research is sponsored by the National Science Foundation.

0021-9991/84 $3.00

especially in the presence of turbulent diffusion, dealing with a shock or discontinuity is not as important as maintaining the positive definiteness of the evaluated scalar quantity. Compromising between computer time efficiency and accuracy, Clark and Hall [4, 5] applied the idea of hybridization to the numerical evaluation of the cloud's water transport equation, developing possibly the simplest known hybrid scheme. The numerical diffusion in this scheme is larger than in the FCT but the time consumption is about half of that in the FCT. Recently developed by Harten [7, 8], the total-variation-diminishing (TVD) schemes, like FCT or SAHS, have been designed to treat shocks and discontinuities. The explicit version of the second-order-accurate TVD scheme [8] is computationally efficient enough to be considered for application in modeling the phenomena mentioned above (in Section 4 of this paper one version of the TVD scheme will be discussed in detail). All FCT, SAHS, and TVD methods have been constructed to maintain monotonicity of the initial condition which implies the maintenance of the positive definiteness of the transported quantity.

This paper presents another solution. Using an iterative approach, one can construct from the basis of the "upstream" scheme a class of nonlinear, multidimensional, positive definite advection transport algorithms with small implicit diffusion. In comparison to the FCT, SAHS, or TVD schemes, the general iterative principle of the algorithm seems to be simple and can be easily developed from the Taylor series expansion applied to the "upstream" scheme [13]. In the first iteration an "upstream" scheme is used in its classical sense, while each following corrective iteration reapplies the "upstream" scheme but with a specially defined "antidiffusive" velocity field. The number of iterations is optional, and each additional iteration increases the solution's accuracy. Such a procedure has been applied successfully in Smolarkiewicz [13] to one-dimensional advection problems and to a multidimensional problem when the scheme has been used in a "time-splitting" form. In a multidimensional case when the scheme was applied to a combined form (the difference between the combined and "time-splitting" forms of the advection schemes was discussed in detail in Smolarkiewicz [12]), only the first corrective iteration gave improved results. The second corrective iteration unrealistically deformed the solution and in some cases even resulted in instability of the scheme. In [13], it was suggested that this error was caused by an effect due to the cross-derivative terms (as was also discussed in detail in [12]). Introducing cross terms to the "antidiffusive" velocities eliminates this problem and results in a fully multidimensional unified algorithm that strictly maintains the positive definiteness of the transported quantity. The proposed algorithm represents an open family of schemes of varying levels of accuracy, complication, and computational efficiency. The simplest version of the scheme is second-order accurate in both space and time. As was shown in [13], it gives results of a quality comparable with that obtained from more complicated hybrid schemes while considerably reducting computational time. The most accurate and complicated version presented in this paper is third-order accurate in time and fifth-order accurate in space. In principle it is possible to construct the algorithm with an optional order of accuracy. For smooth initial conditions the schemes also preserve monotonicity

but for the shock-type initial conditions they may produce locally, in the closest neighbourhood of the shock, a small amplification. This amplification is significantly smaller than the amplitude of oscillation produced by linear schemes of a high order of accuracy and is of minor importance in a broad category of problems. However, the example of the modification of the algorithm for the case of a shock-type initial condition will be discussed as one of the possible options of the scheme.

In Section 2 of this paper the basic form of the algorithm will be developed in general optionally dimensional form. In Section 3 such features of the scheme as consistency, stability, and accuracy will be discussed. Section 4 will present the results of some tests and compare the scheme with a version of the TVD scheme (because the first version of the algorithm was compared with the FCT, SAHS, and Clark and Hall schemes in [13] this comparison will not be repeated here). In Section 5 some of the possible options of the scheme will be discussed.

2. Development of the Algorithm

The equation to be solved is the continuity equation describing transport of the nondiffusive scalar quantity in M-dimensional space (the proposed algorithm was placed in a general M-optional format for compactness, but the author is able to prove the stability of the scheme for $M \leqslant 3$ only, which does not necessarily mean that the scheme is unstable in a case of $M > 3$):

$$\frac{\partial \psi}{\partial t} + \sum_{I=1}^{M} \frac{\partial}{\partial x^I} (\psi u^I) = 0 \tag{1}$$

where $\psi \equiv \psi(t, x^1,..., x^M)$ is the nondiffusive scalar quantity, assumed to be non-negative;

$u^I \equiv u^I(t, x^1,..., x^M)$ is the Ith velocity component, $I = 1,..., M$;

$t, \mathbf{x} \equiv (x^1,..., x^M)$ are the time- and space-independent variables.

To describe compactly the numerical equations that will be used later, it is convenient to introduce a few symbols:

$\psi_{\mathbf{i}}^n$ is a numerical approximation of the solutin of Eq. (1), defined in points $(t^n, \mathbf{x}_{\mathbf{i}})$, where $t^n = n \cdot \Delta t$, $\mathbf{x}_{\mathbf{i}} = (i^1 \Delta X^1, i^2 \Delta X^2,..., i^M \Delta X^M)$, $n = 0,..., NT$; $i^I = 0,..., NX^I$ and ΔX^I is the constant spatial increment in the Ith direction (in this paper the indices described by capital letters, e.g., "I, J," always indicate vector components, and the indices described by lowercase letters, e.g., "i, j," indicate the position on a grid space);

$\mathbf{e}_I \equiv (0, 0,..., 0, 1, 0,..., 0)$ is a unity vector in the Ith direction;

${}^{n}u^{I}_{\mathbf{i}+(1/2)\mathbf{e}_J}$ is the Ith velocity component in the nth time step defined on a staggered grid (the Ith component is staggered $\frac{1}{2}\Delta X^I$ in the Ith direction). Later, to simplify the fomulas, the index "n" beside velocity symbols will be omitted where it is possible to do so without introducing any misunderstandings.

With the above symbols, the well-known first-order-accuracy "upstream" scheme for numerical evaluation of Eq. (1) can be written in the form

$$\psi^{n+1}_{\mathbf{i}} = \psi^{n}_{\mathbf{i}} - \sum_{I=1}^{M} \left[F^I(\psi^{n}_{\mathbf{i}}, \psi^{n}_{\mathbf{i}+\mathbf{e}_I}, u^{I}_{\mathbf{i}+(1/2)\mathbf{e}_I}) - F^I(\psi^{n}_{\mathbf{i}-\mathbf{e}_I}, \psi^{n}_{\mathbf{i}}, u^{I}_{\mathbf{i}-(1/2)\mathbf{e}_I})\right] \tag{2}$$

where F is the advective flux in Ith direction evaluated in the same staggered points as the Ith velocity component and defined as follows:

$$F^I(\psi_{\mathbf{i}}, \psi_{\mathbf{i}+\mathbf{e}_I}, u) \equiv \left[(u + |u|)\,\psi_{\mathbf{i}} + (u - |u|)\,\psi_{\mathbf{i}+\mathbf{e}_I}\right] \frac{\Delta t}{2\,\Delta X^I}. \tag{3}$$

A sufficient stability condition for the scheme in Eq. (2) can be written in the form

$$\forall_{t^n, \mathbf{x}_{\mathbf{i}+(1/2)\mathbf{e}_J}} \sum_{I=1}^{M} |\alpha^{I}_{\mathbf{i}+(1/2)\mathbf{e}_J}| = C_{\mathbf{i}+(1/2)\mathbf{e}_J} \leqslant \mathscr{C} \leqslant 1 \tag{4}$$

(cf. Eqs. (3–140) of Roache [11]), where

$$\alpha^{I}_{\mathbf{i}+(1/2)\mathbf{e}_J} \equiv u^{I}_{\mathbf{i}+(1/2)\mathbf{e}_J} \Delta t / \Delta X^I. \tag{5}$$

Note that originaly u^I was not defined in $\mathbf{x}_{\mathbf{i}+(1/2)\mathbf{e}_J}$ for $I \neq J$ and that this definition is not necessary for numerical evaluation of Eq. (1). For the stability condition it always can be done, at least by the appropriate arithmetical averaging (see, e.g., Eq. (14)). The constant $\mathscr{C} \leqslant 1$ was placed in Eq. (4) to point out that in the case of a divergent flow field, the traditional restriction can be insufficient and (as follows from experience and simple analysis of the behavior of the "upstream" scheme around the point in which each velocity component changes from u^I to $-u^I$) should be replaced by $\mathscr{C} \leqslant \frac{1}{2}$. Under the condition given in (4) the scheme in (2) is positive definite, which means:

$$\left(\forall_{\mathbf{x}_{\mathbf{i}}} \psi^{0}_{\mathbf{i}} \geqslant 0\right) \Rightarrow \left(\forall_{t^n, \mathbf{x}_{\mathbf{i}}} \psi^{n}_{\mathbf{i}} \geqslant 0\right). \tag{6}$$

The properties in Eqs. (4) and (6) of the scheme in Eq. (2), as well as its low computer time consumption, are very useful for the application of Eq. (2) to the numerical evaluation of Eq. (1). Unfortunately, the scheme in Eq. (2) is of first-order accuracy in both time and space and has strong implicit diffusion. The rate of the implicit diffusion may be easily estimated for the case of a uniform flow

($\forall_I u^I = \text{const}$). Expanding ψ_i^{n+1}, $\psi_{i+e_I}^n$, $\psi_{i-e_I}^n$ in a second-order Taylor sum about the point $(t^n, \mathbf{x}_i)$, scheme (2) may be written as

$$\frac{\partial \psi}{\partial t}\Big|_i^n = -\sum_{I=1}^{M} \frac{\partial}{\partial x^I}(u^I \psi)\Big|_i^n + \sum_{I=1}^{M} \frac{\partial}{\partial x^I}\left\{0.5[|u^I|\,\Delta X^I - \Delta t (u^I)^2]\frac{\partial \psi}{\partial x^I} - \sum_{\substack{J=1 \\ J\neq I}}^{M} 0.5\,\Delta t\, u^I u^J \frac{\partial \psi}{\partial x^J}\right\}\Big|_i^n. \tag{7}$$

From Eq. (7) it can be seen that when Δt and $\Delta X^I \to 0$, for all I, Eq. (7) approaches Eq. (1), but during a realistic computational process the scheme in Eq. (2) with finite Δt and ΔX^I approximates more accurately (with second-order accuracy) an advective transport equation with additional diffusive terms rather than the original Eq. (1). On the other hand, these implicit diffusion terms are important for the stability of the scheme and must not be explicitly subtracted from the scheme. An intuitively obvious approach is to make the advection step using Eq. (2) and then reverse the effect of the diffusion equation

$$\frac{\partial \psi}{\partial t} = \sum_{I=1}^{M} \frac{\partial}{\partial x^I}\left\{0.5[|u^I|\,\Delta X^I - \Delta t (u^I)^2]\frac{\partial \psi}{\partial x^I} - \sum_{\substack{J=1 \\ J\neq I}}^{M} 0.5\,\Delta t\, u^I u^J \frac{\partial \psi}{\partial x^J}\right\} \tag{8}$$

in the next corrective step.

The diffusion process and the equation that describes it are irreversible. But this does not mean that the effect of the diffusion process cannot be reversed in time. To do this, one can design a process that will return to the previous state or at least to a state close to it. It is enough to notice that introduction of the artificial "diffusive" velocities u_d^I allows one to write Eq. (8) in the form

$$\frac{\partial \psi}{\partial t} = -\sum_{I=1}^{M} \frac{\partial}{\partial x^I}(u_d^I \psi) \tag{9}$$

where

$$u_d^I = \begin{cases} -0.5[|u^I|\,\Delta X^I - \Delta t (u^I)^2]\dfrac{1}{\psi}\dfrac{\partial \psi}{\partial x^I} \\ \qquad + \displaystyle\sum_{\substack{J=1 \\ J\neq I}}^{M} 0.5\,\Delta t\, u^I u^J \frac{1}{\psi}\frac{\partial \psi}{\partial x^J} & \text{if} \quad \psi > 0 \\ 0 & \text{if} \quad \psi = 0. \end{cases} \tag{10}$$

Now defining "antidiffusive" velocities

$$\tilde{u}^I \equiv -u_d^I \tag{11}$$

the reversal in time of the diffusion equation (8) may be simulated by the advection equation (9) with the "antidiffusive" velocities $\tilde{u}^I$ instead of u_a^I. Based on this concept, the corrective step is suggested in the form

$$\psi_i^{n+1} = \psi_i^* - \sum_{I=1}^{M} [F^I(\psi_i^*, \psi_{i+e_I}^*, \tilde{u}_{i+(1/2)e_I}^I) - F^I(\psi_{i-e_I}^*, \psi_i^*, \tilde{u}_{i-(1/2)e_I}^I)] \tag{12}$$

where ψ_i^* is given by the right-hand side (r.h.s.) of Eq. (2) and

$$\tilde{u}_{i+(1/2)e_I}^I \equiv [|u_{i+(1/2)e_I}^I| \Delta X^I - \Delta t (u_{i+(1/2)e_I}^I)^2] \times \frac{\psi_{i+e_I}^* - \psi_i^*}{(\psi_{i+e_I}^* + \psi_i^* + \varepsilon)\Delta X^I}$$
$$- \sum_{\substack{J=1 \\ J \neq I}}^{M} 0.5 \Delta t \, u_{i+(1/2)e_I}^I \overline{u^J}_{i+(1/2)e_I}$$
$$\times \frac{\psi_{i+e_I+e_J}^* + \psi_{i+e_J}^* - \psi_{i+e_I-e_J}^* - \psi_{i-e_J}^*}{(\psi_{i+e_I+e_J}^* + \psi_{i+e_J}^* + \psi_{i+e_I-e_J}^* + \psi_{i-e_J}^* + \varepsilon)\Delta X^J} \tag{13}$$

where

$$\overline{u^J}_{i+(1/2)e_I} \equiv 0.25(u_{i+e_I+(1/2)e_J}^J + u_{i+(1/2)e_J}^J + u_{i+e_I-(1/2)e_J}^J + u_{i-(1/2)e_J}^J) \tag{14}$$

and ε is a small value, e.g., 10^{-15}, to ensure $\tilde{u}^I = 0$ when $\psi_{i+e_I}^* = \psi_i^* = 0$ or $\psi_{i+e_I+e_J}^* = \psi_{i+e_J}^* = \psi_{i+e_I-e_J}^* = \psi_{i-e_J}^* = 0$. The corrective step is again the "upstream" scheme and also contains implicit diffusion that again can be corrected by the next corrective step. The number of corrective steps is optional, so the final algorithm may be written in the form

$$\psi_i^{(*)^k} = \psi_i^{(*)^{k-1}} - \sum_{I=1}^{M} [F^I(\psi_i^{(*)^{k-1}}, \psi_{i+e_I}^{(*)^{k-1}}, \overset{(\sim)^k}{u}{}_{i+(1/2)e_I}^I)$$
$$- F^I(\psi_{i-e_I}^{(*)^{k-1}}, \psi_i^{(*)^{k-1}}, \overset{(\sim)^k}{u}{}_{i-(1/2)e_I}^I)] \tag{15}$$

where $k = 1,\ldots,$ IORD; ${}^{(\tilde{u})^{k+1}} = \tilde{u}({}^{(\tilde{u})^k}, \psi^{(*)^k})$ evaluated from Eqs. (13) and (14) and $\psi_i^{(*)^0} \equiv \psi_i^n$, $\psi_i^{(*)^{\mathrm{IORD}}} \equiv \psi_i^{n+1}$, $\overset{(\sim)^1}{u}{}_{i+(1/2)e_I}^I \equiv {}^n u_{i+(1/2)e_I}^I$. Note that when IORD = 1 the algorithm in Eq. (15) is exactly the same as the classical "upstream" scheme. Theoretically IORD may be any value, but, as can be concluded from the performed tests, using IORD > 4 only negligibly improves the accuracy of the solution while increasing the computational costs of the scheme. In [13] the second term in Eq. (13), which compensates the effect of the cross-spatial derivatives in Eq. (7), was not evaluated. In a multidimensional case for IORD > 2, this neglect resulted in deformation of the solution or even in instability of the scheme.

3. Consistency, Stability, and Accuracy of the Algorithm

The proposed algorithm is constructed from the well-known, conditionally stable, and consistent "upstream" scheme. To show the consistency of the entire scheme in Eq. (15) it is enough to show that when $\Delta t, \Delta X^I \to 0$, for all I, the corrective iterations ($k > 1$ in Eq. (15)) do not affect the solution of the first iteration ($k = 1$ in Eq. 15). From Eqs. (13), (11), and (10) it is easy to see that when $\Delta t, \Delta X^I \to 0$ then $\tilde{u}^I_{i+(1/2)\mathbf{e}_I} \to 0$, which implies $\overset{(\sim)^k}{u}{}^I_{i+(1/2)\mathbf{e}_I} \to 0$ for all k. The latter implies that Eq. (15) for $k > 1$ converges to

$$\frac{\partial \psi}{\partial t} = 0 \tag{16}$$

which means that the scheme is consistent.

To show the stability of the scheme it is enough to show that stability of the first iteration implies stability of all subsequent iterations. An optional grid point and time step may be taken into consideration to prove stability for any arbitrary grid point and time step. The notation is simplified for this analysis by omitting the indices that indicate the position on the grid space. The application of Eq. (13) results in

$$\tilde{\alpha}^I = (|\alpha^I| - (\alpha^I)^2)\,\xi^I - \tfrac{1}{2} \sum_{\substack{J=1 \\ J \neq I}}^{M} \alpha^I \alpha^J \beta^{IJ} \tag{17}$$

where $\tilde{\alpha}^I$ is related to $\tilde{u}^I$, as in Eq. (5), and ξ^I and β^{IJ} are the $\Delta\psi^*/\psi^*$ ratios in Eq. (13). Because all ψ^* values have been obtained from the positive definite "upstream" scheme, $\forall_{I,J} |\xi^I|, |\beta^{IJ}| \leqslant 1$. Because of Eq. (4), $\forall_I |\alpha^I| \leqslant \mathscr{C} \leqslant 1$, which implies $0 \leqslant |\alpha^I| - (\alpha^I)^2 \leqslant 0.25$ in Eq. (17). Using this information, it can be shown that

$$|\tilde{\alpha}^I| \leqslant |\alpha^I| - (\alpha^I)^2 + \tfrac{1}{2} |\alpha^I| \sum_{\substack{J=1 \\ J \neq I}}^{M} |\alpha^J|. \tag{18}$$

Because of Eq. (4)

$$\sum_{J=1}^{M} |\alpha^J| = C. \tag{19}$$

The sum of Eq. (18) over all I and the use of Eq. (19) lead to

$$\sum_{I=1}^{M} |\tilde{\alpha}^I| \leqslant C + \tfrac{1}{2} C^2 - \tfrac{3}{2} \sum_{I=1}^{M} |\alpha^I|^2. \tag{20}$$

From the Schwartz's inequality,

$$\sum_{I=1}^{M} |\alpha^I|^2 \geqslant C^2/M \tag{21}$$

which allows us to write Eq. (20) in the form

$$\sum_{I=1}^{M} |\tilde{\alpha}^I| \leqslant C + \tfrac{1}{2} C^2((M-3)/M). \tag{22}$$

The r.h.s. of the inequality in (22) is less than or equal to C for $M \leqslant 3$ so finally

$$\forall_{t^n, \mathbf{x}_{\mathbf{i}+(1/2)\mathbf{e}_j}, M \leqslant 3} \sum_{I=1}^{M} |\tilde{\alpha}^I_{\mathbf{i}+(1/2)\mathbf{e}_j}| \leqslant \sum_{I=1}^{M} |\alpha^I_{\mathbf{i}+(1/2)\mathbf{e}_j}| \tag{23}$$

which results in

$$\forall_{t^n, \mathbf{x}_{\mathbf{i}+(1/2)\mathbf{e}_j}, M \leqslant 3} \sum_{I=1}^{M} |\overset{(\sim)^{k+1}}{\alpha^I_{\mathbf{i}+(1/2)\mathbf{e}_j}}| \leqslant \sum_{I=1}^{M} |\overset{(\sim)^{k}}{\alpha^I_{\mathbf{i}+(1/2)\mathbf{e}_j}}|. \tag{24}$$

Additionally, the maximum values of the r.h.s. of Eq. (22) are $\frac{1}{4}$, $\frac{1}{2}$, and C for $M = 1$, 2, and 3, respectively. This is an important conclusion because even if the original velocity field is nondivergent the "antidiffusive" velocity field is divergent. So, to be positive that the whole scheme is stable, it is safer to ensure that te r.h.s. of Eq. (24) is less than or equal to $\frac{1}{2}$. Finally, we have proved that for $M = 1, 2$ the stability of the first iteration implies the stability of the whole scheme, and for $M = 3$ this is true if the constant $\mathscr{C}$ in Eq. (4) is less than or equal to $\frac{1}{2}$. The performed tests, e.g., $M = 3$ and $\mathscr{C} = 0.95$, suggest that the algorithm is always stable if the original "upstream" scheme is stable, but this conclusion is still unproved for $M \geqslant 3$.

Because each iteration of the algorithm is in the form of the "upstream" scheme, fulfilling the stability criteria ensures that the scheme is positive definite.

The scheme is nonlinear even in the case of a uniform velocity field. According to Harten [8, p. 6], stability and consistency are the only necessary conditions for its convergence. From Eqs. (12) and (13) it is easy to see that when $\Delta t, \Delta X^I \to 0$, for all I, the scheme converges to an "upstream" scheme. The latter point, as well as the results of the performed tests, suggests that convergence of the scheme is at least as well ensured as for the "upstream" scheme.

The algorithm's order of accuracy can be determined by estimating the truncation error. It can be shown and confirmed by the results of tests that the scheme is at least second-order-accurate in space. When time dependence of the velocity field can be ignored the scheme is also second-order-accurate in time. Let's assume for the sake of simplicity that the considered scheme has IORD = 2 and that the specified velocity field is time independent and nondivergent. Although for development of Eq. (7) a uniform velocity field has been assumed it is easy to show that to obtain Eq. (7) it is enough to assume a nondivergent velocity field (in Section 5 of this paper it will be

shown how to generalize the scheme for a divergent velocity field case). To simplify the calculation it will be assumed that $M = 1$ in (1). Under these assumptions ψ^*, given by the first iteration of the scheme, is a second-order-accurate solution of Eq. (7), and can be written in the form

$$\psi^* = \psi^n - \int_{t^n}^{t^n+\Delta t} \frac{\partial}{\partial x}(u\psi)\,dt + \frac{(\Delta X)^2}{\Delta t}\int_{t^n}^{t^n+\Delta t} \frac{\partial}{\partial x} K_\alpha \frac{\partial \psi}{\partial x}\,dt + 0^2(\Delta X, \Delta t)\,\Delta t \quad (25)$$

where $K_\alpha \equiv \frac{1}{2}(|\alpha| - \alpha^2)$, $\alpha = u\,\Delta t/\Delta X$, and $0^2(\Delta X, \Delta t)$ is a second-order small term ΔX, Δt dependent. Similarly ψ^{n+1}, given by the second iteration of the scheme, is a second-order-accurate solution of Eq. (7) with ψ^*, $\tilde{u}$ instead of ψ, u, which can be written in the form

$$\psi^{n+1} = \psi^* - \int_{t^n}^{t^n+\Delta t} \frac{\partial}{\partial x}(\tilde{u}\psi^*)\,d\tau + \frac{(\Delta X)^4}{\Delta t}\int_{t^n}^{t^n+\Delta t} \frac{\partial}{\partial x} K_{\tilde{\alpha}} \frac{\partial \psi^*}{\partial x}\,d\tau + 0^2(\Delta X, \Delta t)\,\Delta t \quad (26)$$

where $K_{\tilde{\alpha}} = K_\alpha - 2K_\alpha^2$. From Eq. (13),

$$\tilde{u} = \frac{(\Delta X)^2}{\Delta t} K_\alpha \frac{1}{\psi^*}\frac{\partial \psi^*}{\partial x} + 0^2(\Delta X, \Delta t). \quad (27)$$

After using Eqs. (25) and (27) in (26) and omitting the third term of the r.h.s. of (26) as a higher-order small term, Eq. (26) can be written in a form

$$\begin{aligned}\psi^{n+1} = \psi^n &- \int_{t^n}^{t^n+\Delta t} \frac{\partial}{\partial x}(u\psi)\,dt + \frac{(\Delta X)^2}{\Delta t}\int_{t^n}^{t^n+\Delta t} \frac{\partial}{\partial x} K_\alpha \frac{\partial \psi}{\partial x}\,dt \\ &- \frac{(\Delta X)^2}{\Delta t}\int_{t^n}^{t^n+\Delta t} \frac{\partial}{\partial x} K_\alpha \frac{\partial \psi}{\partial x}\,d\tau \\ &+ \frac{(\Delta X)^2}{\Delta t}\int_{t^n}^{t^n+\Delta t} \frac{\partial}{\partial x} K_\alpha \frac{\partial}{\partial x}\left|\int_{t^n}^{t^n+\Delta t} \frac{\partial}{\partial x}(u\psi)\,dt\right. \\ &+ \left.\frac{(\Delta X)^2}{\Delta t}\int_{t^n}^{t^n+\Delta t} \frac{\partial}{\partial x} K_\alpha \frac{\partial \psi}{\partial x}\,dt\right| d\tau + 0^2(\Delta X, \Delta t)\,\Delta t. \end{aligned} \quad (28)$$

Note that the first-order small diffusive terms compensate each other and Eq. (28) may be rewritten as

$$\begin{aligned}\psi^{n+1} = \psi^n &- \int_{t^n}^{t^n+\Delta t} \frac{\partial}{\partial x}(u\psi)\,dt \\ &+ \frac{(\Delta X)^2}{\Delta t}\int_{t^n}^{t^n+\Delta t} \frac{\partial}{\partial x} K_\alpha \frac{\partial}{\partial x}\left(\int_{t^n}^{t^n+\Delta t}(u\psi)\,dt\right) d\tau \\ &+ 0^2(\Delta X, \Delta t)\,\Delta t. \end{aligned} \quad (29)$$

Because the third term on the r.h.s. of (29) is of the leading order $(\Delta X)^2\,\Delta t$, Eq. (29) may be finally written in the form

$$\psi^{n+1} = \psi^n - \int_{t^n}^{t^n+\Delta t} \frac{\partial}{\partial x}(u\psi)\,dt + 0^2(\Delta X, \Delta t)\,\Delta t \tag{30}$$

which means that ψ^{n+1} is a solution of Eq. (1) that is second-order-accurate in time and space. The same conclusion could be reached in a more heuristic manner. It is enough to note that the corrective step compensates the first-order small diffusive term with the accuracy to the first order of the first-order small term. This means that the residual of the compensation is a second-order small term. It is still unclear whether increasing the number of iterations increases the order of accuracy of the scheme or only decreases the amplitude of the existing $0^2(\Delta X, \Delta t)\,\Delta t$ error in (30).

From Eqs. (13) and (15) it can be concluded that a two-iteration scheme (IORD = 2) results in a three-point scheme while a three-iteration scheme

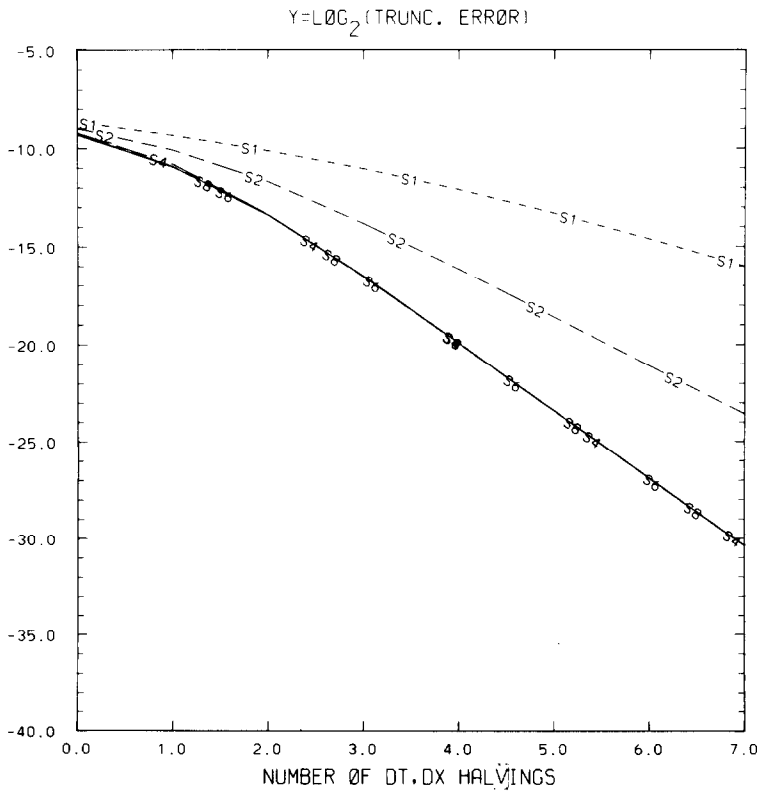

FIG. 1. The dependence of the measure of the truncation error on the number of halvings of the grid and time increments. The curves $S1$–$S8$ represent schemes with IORD = 1–8, respectively.

(IORD = 3) results in a five-point scheme. Generally an IORD-iteration scheme determines gradients of fluxes on the basis of the information from 2 · IORD–1 points. To illustrate the behavior of the truncation error the following test has been performed. In a uniform one-dimensional velocity field the initial condition in the form of the Gauss-type function has been assumed. After an arbitrarily chosen fixed time period, $T = NT \cdot \Delta t$, the average error per time and per space step between the numerical and analytical solutions has been evaluated as follows:

$$\mathrm{TRER}(NT, NX) \equiv \left[\sum_{i=1}^{NX} (\psi(T, x_i) - \psi_i^{NT})^2 / (NT \cdot NX) \right]^{1/2} \tag{31}$$

where $\psi(T, x_i)$, ψ_i^{NT} are the analytical and numerical solutions, respectively, at the point (T, x_i). Dividing successively Δt, ΔX by 2 and doubling simultaneously NT, NX, the sequence of $\mathrm{TRER}(NT, NX)$ has been obtained. The dependence of the $\log_2(\mathrm{TRER})$ on the number of halvings of the original Δt, ΔX is presented in Fig. 1 for different IORD's and the chosen Courant number 0.5. The curves $S1$, $S2$, $S4$, $S6$,

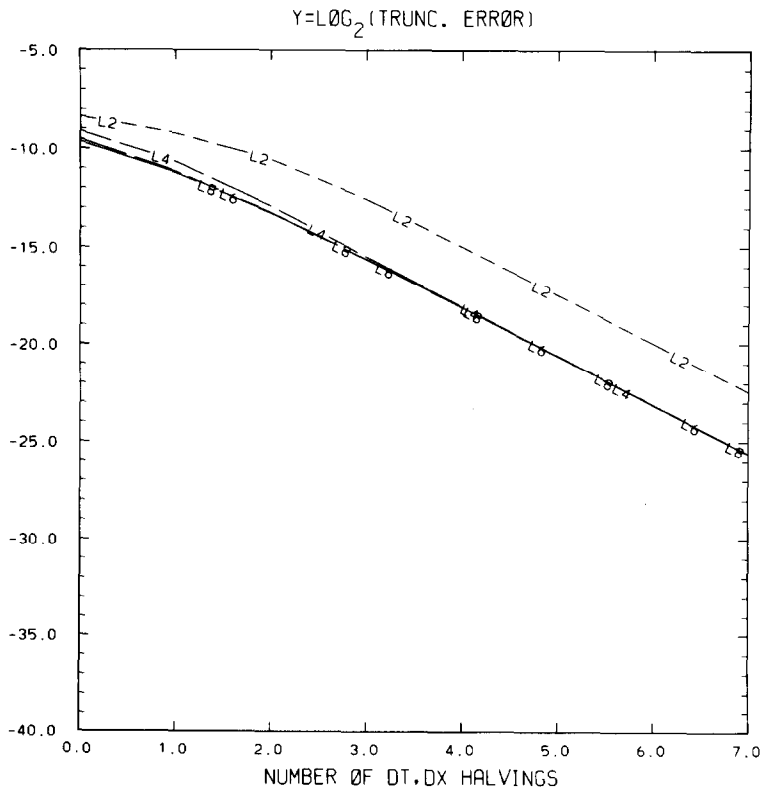

FIG. 2. As in Fig. 1 but for a leapfrog-trapezoidal scheme second-order-accurate in time and second- ($L2$) to eight- ($L8$) order accurate in space.

and $S8$ are equivalent to IORD = 1, 2, 4, 6, and 8, respectively. In Fig. 2 the same dependence is presented but for the well-known leapfrog-trapezoidal scheme (Zalesak [14, Appendix]), which is second-order-accurate in time and second-, fourth-, sixth-, and eighth-order-accurate in space. The curves $L2$, $L4$, $L6$, and $L8$ represent the different versions of the leapfrog scheme. Note that the quantity TRER defined in Eq. (31) does not represent the truncation error according to its definition [10, p. 20] but rather some measure of that error. So, the order of the accuracy of the various schemes cannot be estimated directly from the plots presented in Figs. 1 and 2. Generally the truncation error may be written in the form

$$\text{truncation error} \sim (\Delta t)^{\rho_t}(C_1 + C_2(\Delta X)^{\rho_x - \rho_t} + \cdots) \tag{32}$$

where ρ_t, ρ_x are the leading orders of the truncation in time and space, respectively, and C_1, C_2 are coefficients that are generally solution and Courant number

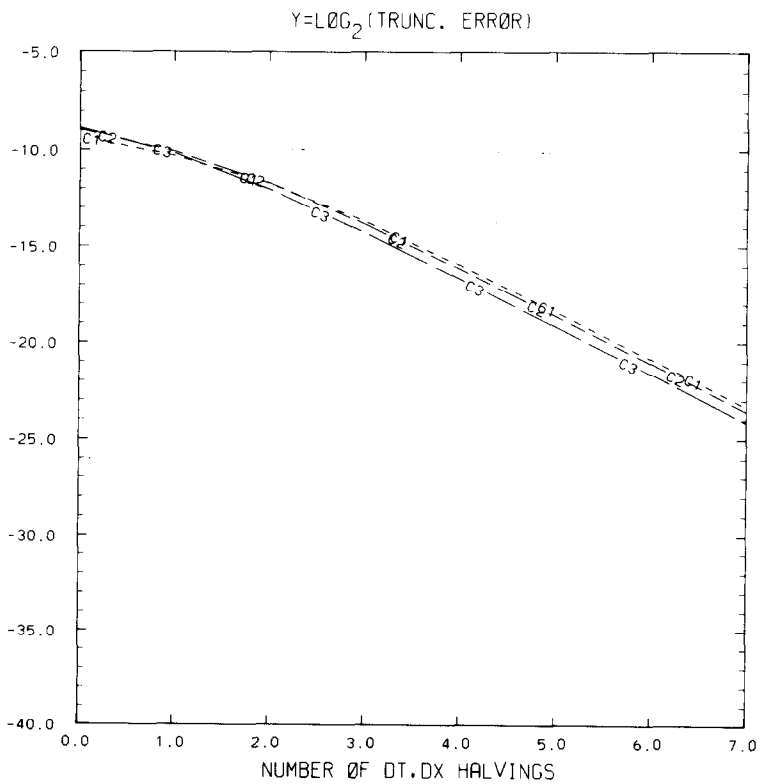

FIG. 3. As in Fig. 1 but for an IORD = 2 scheme. Curves $C1$, $C2$, and $C3$ are for CFL = 0.25, 0.5, and 0.75, respectively.

dependent. From (32) it can be seen that when $\Delta t = 2^{-n}\,\Delta t_0$, $\Delta X = 2^{-n}\,\Delta X_0$, and n is "big," then

$$\log_2 (\text{tr. error}) \sim -\rho_t n + \begin{cases} \log_2(C_1 + C_2) & \text{if } \rho_x = \rho_t \\ \log_2 C_1 & \text{if } \rho_x > \rho_t. \end{cases} \tag{33}$$

The relation in (33) explains the shape of the curves in Figs. 1 and 2. Note that for a "big" n all lines $L2$–$L8$ have the same slope, and the lines $L4$–$L8$ are identical. Generally it can be concluded that the slopes of the lines in Figs. 1 and 2 illustrate the order of truncation error in time while the shift between the lines for the same type of scheme is related to the order of the truncation in space. Comparing $S2$ with $L2$ and $S4$–$S8$ with $L4$–$L8$ in Figs. 1 and 2, it can be seen that $S2$ has the same slope as $L2$ and lies entirely below $L2$ while $S4$–$S8$ have greater slopes than $L4$–$L8$ and lie entirely below them. To make a final conclusion it is necessary to present the dependence of the TRER quantity on the Courant number. In Figs. 3 and 4 the two-

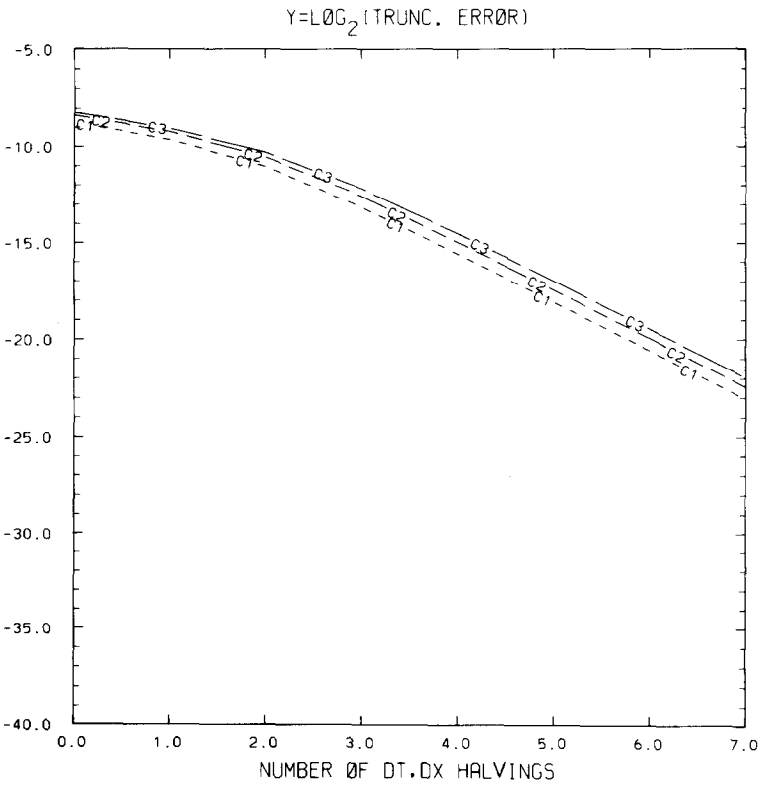

FIG. 4. As in Fig. 3 but for a leapfrog-trapezoidal scheme second-order-accurate in both time and space.

iteration scheme and second-order in the time and space leapfrog scheme are compared for Courant numbers $C1 = 0.25$, $C2 = 0.5$, and $C3 = 0.75$. From Figs. 3 and 4 it can be seen that for all Courant numbers the lines for the two-iteration scheme have the same slopes as the lines for the leapfrog scheme. It also can be seen that the curves in Fig. 3 lie entirely below the curves in Fig. 4. These features suggest that the two-iteration scheme is second-order-accurate in time and space. In Figs. 5 and 6 the same comparison is presented for a four-iteration scheme and a second-order accuracy in time and fourth-order accuracy in space leapfrog scheme. Comparing Figs. 1, 2, and 5, it can be concluded that the greater slope for $S4$–$S8$ than for $L4$–$L8$ does not indicate a difference in order of accuracy in time between, say, $S4$ and $L4$ but rather some particular dependence of the truncation error on the Courant number. Comparing Figs. 5 and 6 it can be noticed that the values of TRER for the four-iteration scheme are smaller than those for the 2/4-leapfrog scheme but have a different dependence on the Courant number. Note that $C1$ in Fig. 5 lies above $C1$ but below $C3$ in Fig. 6. This suggests that the four-iteration scheme is fourth-

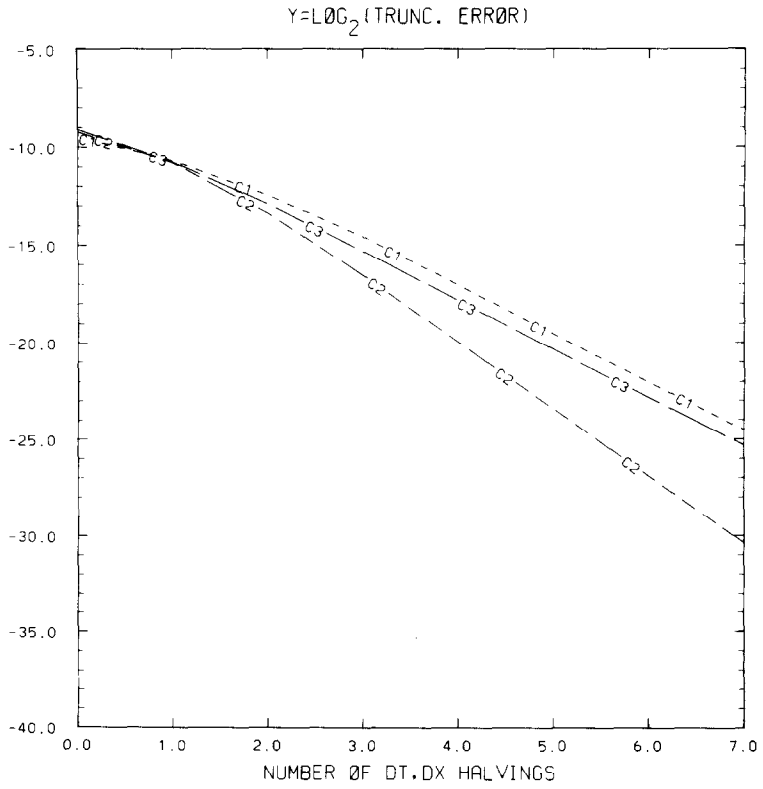

FIG. 5. As in Fig. 3 but for an IORD = 4 scheme.

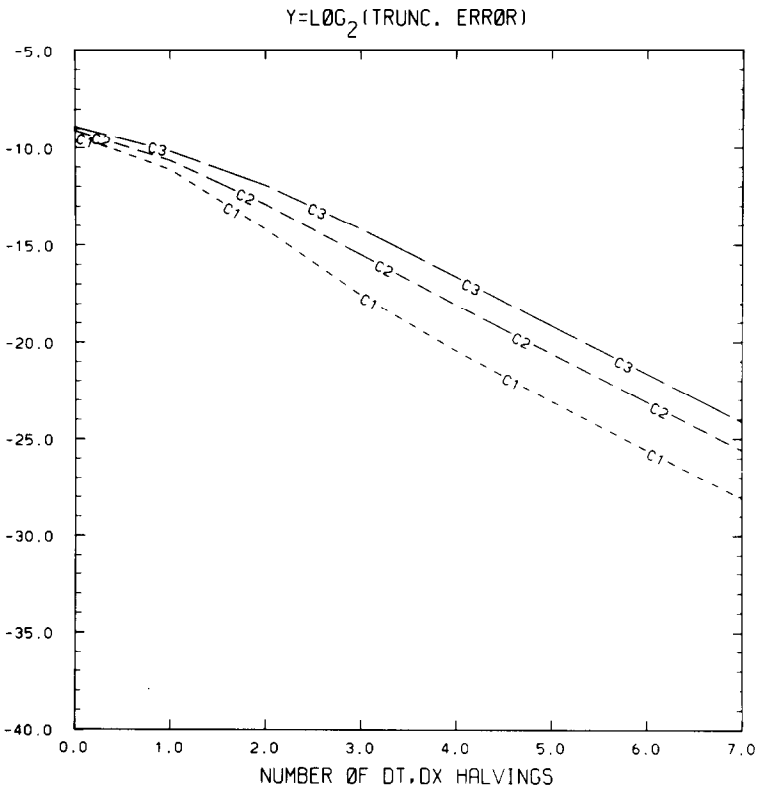

FIG. 6. As in Fig. 3 but for a leapfrog-trapezoidal scheme second-order-accurate in time and fourth-order-accurate in space.

order-accurate in space and generally that increasing the number of iterations increases the order of accuracy in space. It also can be concluded that the truncation error reaches a minimum for Courant number 0.5.

4. RESULTS OF TESTS

Two- and three-dimensional solid-body rotation tests were performed to illustrate the behavior of the proposed algorithm. The one-dimensional version of the scheme was tested in [13]. The two-dimensional case used 101 points in each direction with $\Delta X^1 = \Delta X^2 = \Delta X = 1$, $\Delta t = 0.1$, and a constant angular velocity of $\omega = 0.1$. The velocity components are $u^1 = -\omega(x^2 - xo^2)$ and $u^2 = \omega(x^1 - xo^1)$, where $(xo^1, xo^2) = (50\,\Delta X, 50\,\Delta X)$. One full rotation around the point (xo^1, xo^2) was equivalent to 628 time steps. In this circumstance the constant $\mathscr{C}$ in the stability criterion (4) was 0.99. A cone was used as the initial condition with a base radius of

$15\,\Delta X$ and a maximum value of 4.0 at the point $(xm^1, xm^2) = (75\,\Delta X, 50\,\Delta X)$ (Fig. 7). For all tests performed the same boundary conditions were used. The first partial spatial derivative in the normal direction was assumed to vanish at the outflow boundary (vanishing of the second derivative does not ensure the positive definiteness of the scheme). The undisturbed value of the field was assumed at the inflow boundary. The solution after six full rotations (3768 time steps) is presented in Figs. 8, 9, and 10 for the scheme in Eq. (15) with IORD = 2, 3, and 4, respectively. The maximal values of the presented solutions are 2.16, 3.17, and 3.25, respectively, and the "energy" error ER2 is 0.52, 0.20, and 0.14, where ER2 is defined as

$$ER2 \equiv 1 - \left\{ \int_\sigma \psi^2(x^1, x^2, t)\, dx^1\, dx^2 + \int_0^t |\text{outflow}(\psi^2)\, dt| \right\} \times \left\{ \int_\sigma \psi^2(x^1, x^2, 0)\, dx^1\, dx^2 \right\}^{-1} \tag{34}$$

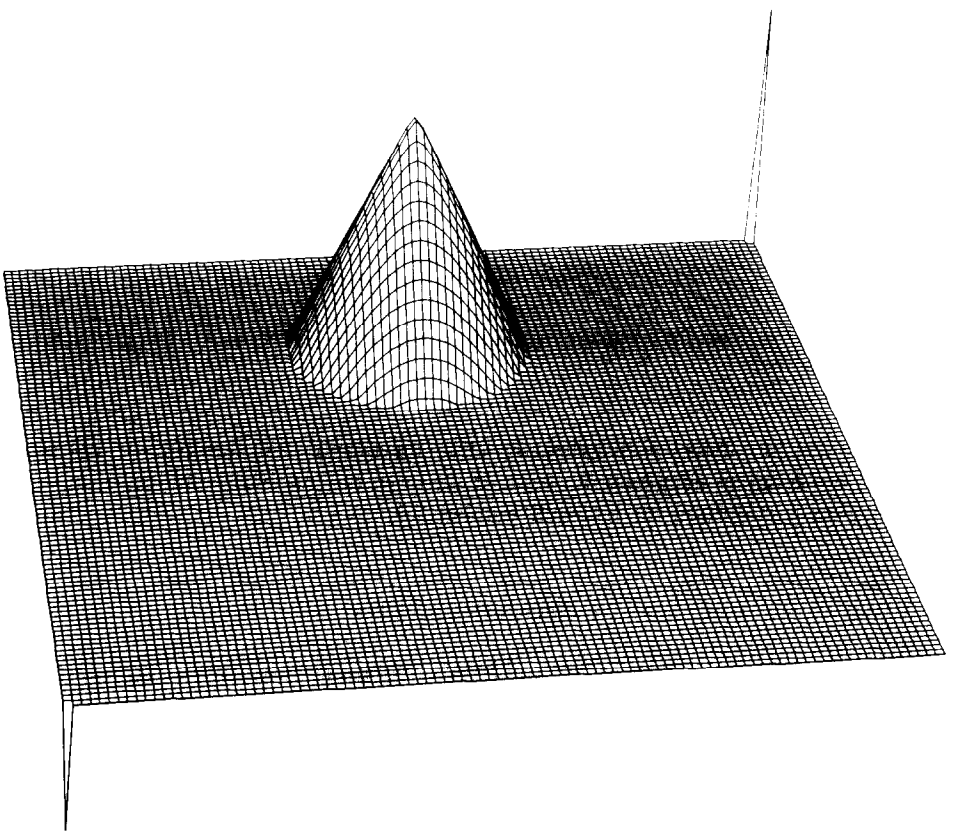

FIG. 7. Initial condition for the two-dimensional tests. The scale values in left-front and right-back corners are −2 and 4, respectively. The scale values are the same in all figures.

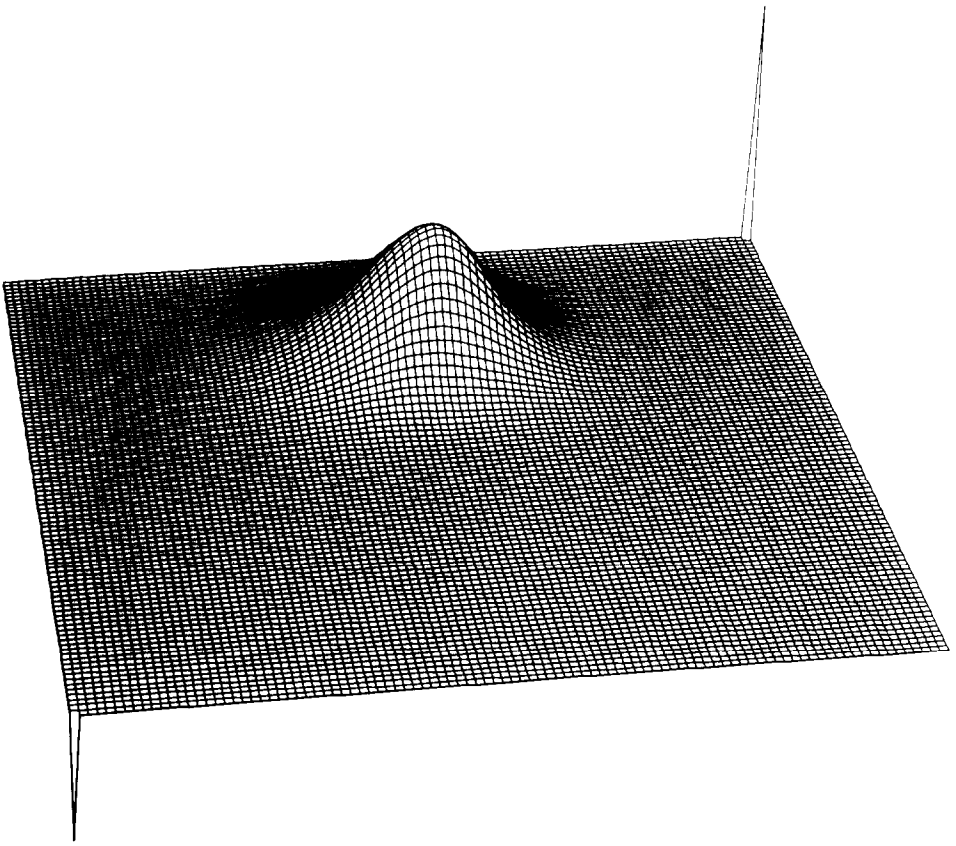

FIG. 8. Solution for an IORD = 2 scheme after six full rotations (3768) time steps.

where σ signifies the whole domain of x^1, x^2. All versions of the scheme that were considered are in a conservative form, and the error of the conservation of ψ was to a roundoff error level of 10^{-12}. Furthermore, the minimum value of the solution obtained was 0. It can be seen, by comparing Figs. 8, 9, and 10 and taking into consideration that when a simple "upstream" scheme (IORD = 1) is used the solution almost vanishes [13, Fig. 2], that significant improvements of the algorithm's accuracy are obtained when IORD changes between 1 and 4. For IORD > 4 the differences between two successive IORD schemes are unnoticeable on the figures, e.g., for IORD = 6 the maximum value of the tested solution is 3.27 and ER2 is 0.12. When the results presented in Figs. 8, 9, and 10 are compared with the equivalent results obtained from the time-splitting form of the one-dimensional version of the scheme [13, Figs. 13, 14, and 15] it can be concluded that the combined form of time-differencing gives slightly better results than time-splitting. The results shown in Figs. 8, 9, and 10 have been compared with the solutions obtained from the second-

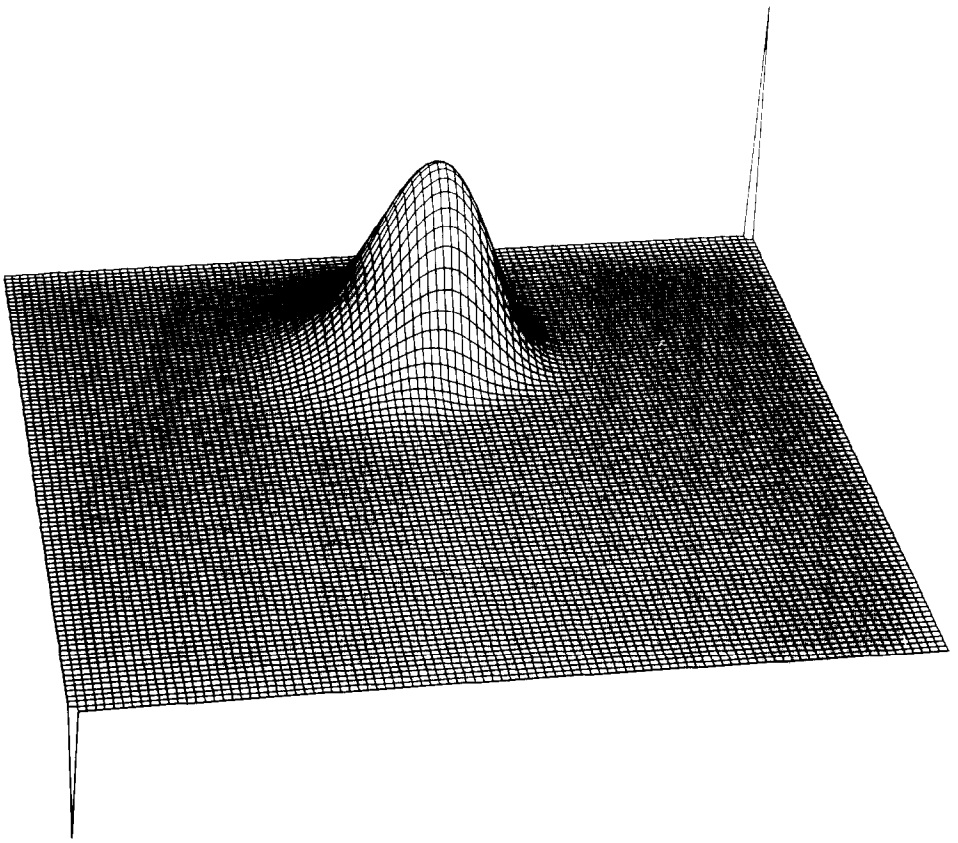

FIG. 9. As in Fig. 8 but for an IORD = 3 scheme.

order-accurate explicit version of the TVD scheme [8, following Theorem 4.3 and Eqs. (3.5) with $\eta = 0$, (3.10), (3.16b) with $\varepsilon = 0$, (4.1), (4.5), (4.8) with $\hat{g} = 0$]. Figure 11 shows the solution after six rotations for the time-splitting form of the chosen version of the TVD scheme. Solution maximum and ER2 values are 1.63 and 0.52, respectively. In Fig. 12a the same solution is presented, but for the scheme applied in a combined time-differencing form. Solution maximum and ER2 are 1.52 and 0.60. Comparing Fig. 12a with Fig. 11, it can be seen that the combined form of the scheme results in a deformation of the solution (elongation normal to the direction of motion); this is especially clear in Fig. 12b, where the solution is shown a quarter of a rotation earlier than in Fig. 12a. This deformation is typical for all multidimensional higher-order schemes that do not take into account the cross-spatial-partial derivatives [12, 13]. It can also be concluded that the chosen version of the TVD scheme is even more diffusive than the IORD = 2 version of the proposed algorithm. Computer time consumption for both schemes is practically the

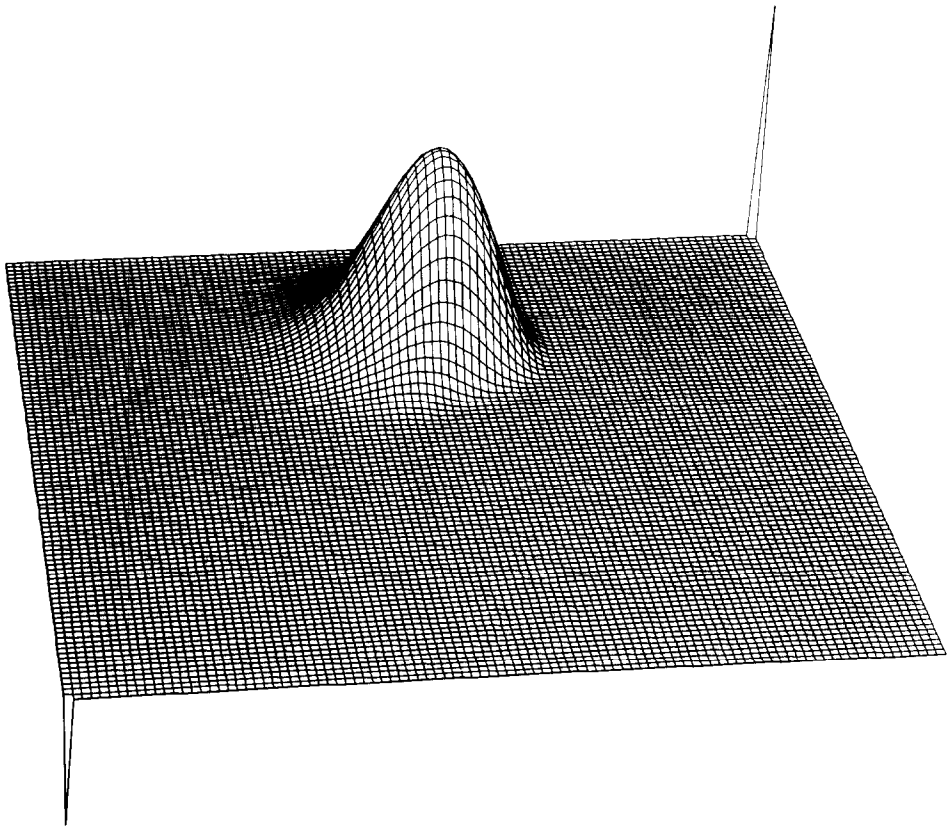

FIG. 10. As in Fig. 8 but for an IORD = 4 scheme.

same, i.e., about three times that required for the simple "upstream" scheme. For versions of the scheme with IORD = 3 and 4, computer time consumption is about five and seven times that required for the "upstream" scheme. Compare this with the FCT scheme [13], which requires about eight times the "upstream" amount.

In the three-dimensional case the number of grid points chosen was 41 in each direction with $\Delta X^1 = \Delta X^2 = \Delta X^3 = \Delta X = 2.5$, $\Delta t = 0.2$, and a constant angular velocity $\Omega = (\omega/2, \omega/2, \omega(2)^{-1/2})$, where $\omega = 0.1$. The velocity components are $u^1 = -\Omega^3(x^2 - xo^2) + \Omega^2(x^3 - xo^3)$, $u^2 = \Omega^3(x^1 - xo^1) - \Omega^1(x^3 - xo^3)$, and $u^3 = -\Omega^2(x^1 - xo^1) + \Omega^1(x^2 - xo^2)$, where $(xo^1, xo^2, xo^3) = (20\,\Delta X, 20\,\Delta X, 20\,\Delta X)$. The initial condition was a sphere with the radius $7\,\Delta X$ and linearly variable density from 0 on the edge to a maximum value of 4 in the center $(20\,\Delta X - 7\,\Delta X(6)^{-1/2}$, $20\,\Delta X - 7\,\Delta X(6)^{-1/2}$, $20\,\Delta X + 14\,\Delta X(6)^{-1/2})$. In Fig. 13 the values greater than or equal to 0.5 are plotted. The sphere is rotating around the diagonal axis of the grid space that passes through the corner shown in Fig. 13. One full revolution around the

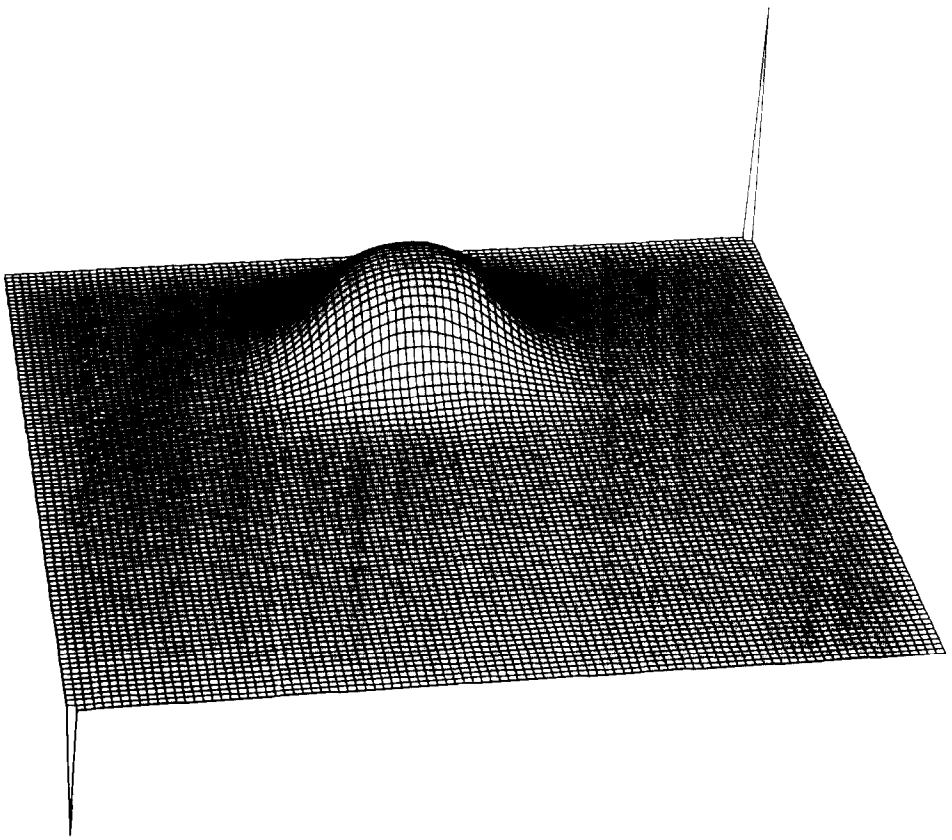

FIG. 11. As in Fig. 8 but for the time-splitting version of the TVD scheme.

point (xo^1, xo^2, xo^3) is equivalent to 314 time steps. The maximum value of the Courant number $\mathscr{C}$ in the stability condition (4) is 0.95. In Figs. 14 and 15 the values greater than or equal to 0.5 of the solutions after five revolutions are shown for the four-iteration scheme (15) and time-splitting TVD scheme, respectively. The maximum solution values are 1.67 and 0.55 and the ER2's are 0.63 and 0.88, respectively, for both schemes. The results for the combined form of the TVD scheme are not presented because the maximum solution value is $\lesssim 0.50$ (ER2 = 0.91). From Fig. 14 it can be seen that the solution is deformed, i.e., elongated toward the center of the rotation. Because similar difficulties in a two-dimensional advective transport problem have been solved by introducing the second-order cross terms explicitly to the scheme, it was suspected that taking into account the third-order cross terms would solve "deformation trouble" in a three-dimensional case. Repeating the whole procedure discussed in Section 2 but applying the third-order Taylor series expansion

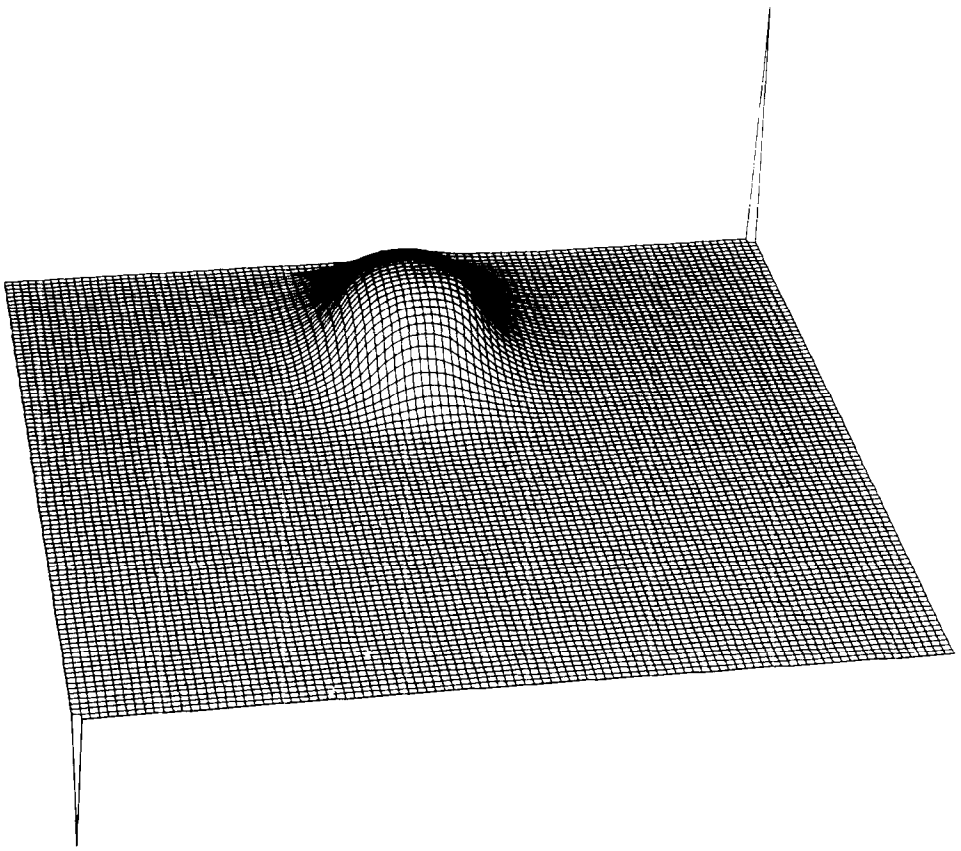

FIG. 12a. As in Fig. 8 but for the combined version of the TVD scheme.

instead of the second-order one leads to a corrected form of the "antidiffusive" velocity:

$$\tilde{u}^I_{i+(1/2)\mathbf{e}_I} = (\tilde{u}^I_{i+(1/2)\mathbf{e}_I})_{\text{Eq.(13)}} + \hat{u}^I_{i+(1/2)\mathbf{e}_I} \tag{35}$$

where

$$\hat{u}^I_{i+(1/2)\mathbf{e}_I} = -\frac{1}{3}\,(u^I_{i+(1/2)\mathbf{e}_I}(\Delta X^I)^2 - (u^I_{i+(1/2)\mathbf{e}_I})^3\,\Delta t^2)$$
$$\times \frac{(\psi^*_{i-\mathbf{e}_I} - \psi^*_i - \psi^*_{i+\mathbf{e}_I} + \psi^*_{i+2\mathbf{e}_I})}{(\text{sum of the above terms} + \varepsilon)(\Delta X^I)^2}$$
$$+ \sum_{\substack{J=1 \\ J\neq I}}^{M} \Delta t^2 (u^I_{i+(1/2)\mathbf{e}_I})^2\, \overline{u^J}_{i+(1/2)\mathbf{e}_I}$$

$$\times \frac{(\psi^*_{\mathbf{i}+\mathbf{e}_I+\mathbf{e}_J} - \psi^*_{\mathbf{i}+\mathbf{e}_I-\mathbf{e}_J} - \psi^*_{\mathbf{i}+\mathbf{e}_J} - \psi^*_{\mathbf{i}-\mathbf{e}_J})}{(\text{sum of the above terms} + \varepsilon)\,\Delta X^I\,\Delta X^J}$$

$$+ \frac{1}{3} \sum_{\substack{J=1 \\ J\neq I}}^{M} u^I_{\mathbf{i}+(1/2)\mathbf{e}_I} \bar{u}^J_{\mathbf{i}+(1/2)\mathbf{e}_I} \sum_{\substack{L=1 \\ L\neq J\neq I}}^{M} \bar{u}^L_{\mathbf{i}+(1/2)\mathbf{e}_I}$$

$$\times \frac{\begin{array}{c}\psi^*_{\mathbf{i}+\mathbf{e}_J+\mathbf{e}_L} - \psi^*_{\mathbf{i}-\mathbf{e}_J+\mathbf{e}_L} - \psi^*_{\mathbf{i}+\mathbf{e}_J-\mathbf{e}_L} + \psi^*_{\mathbf{i}-\mathbf{e}_J-\mathbf{e}_L} + \psi^*_{\mathbf{i}+\mathbf{e}_I+\mathbf{e}_L+\mathbf{e}_J} \\ - \psi^*_{\mathbf{i}+\mathbf{e}_I+\mathbf{e}_L-\mathbf{e}_J} - \psi^*_{\mathbf{i}+\mathbf{e}_I+\mathbf{e}_J-\mathbf{e}_L} - \psi^*_{\mathbf{i}+\mathbf{e}_I-\mathbf{e}_J-\mathbf{e}_L}\end{array}}{(\text{sum of the above terms} + \varepsilon)\,\Delta X^J\,\Delta X^L}. \tag{36}$$

Note that the structure of the scheme remains the same as in Eq. (15) and only new terms are included in the "antidiffusive" velocities. Extending the results of Section 3 it can be concluded that this newly obtained version of the algorithm is third-order-

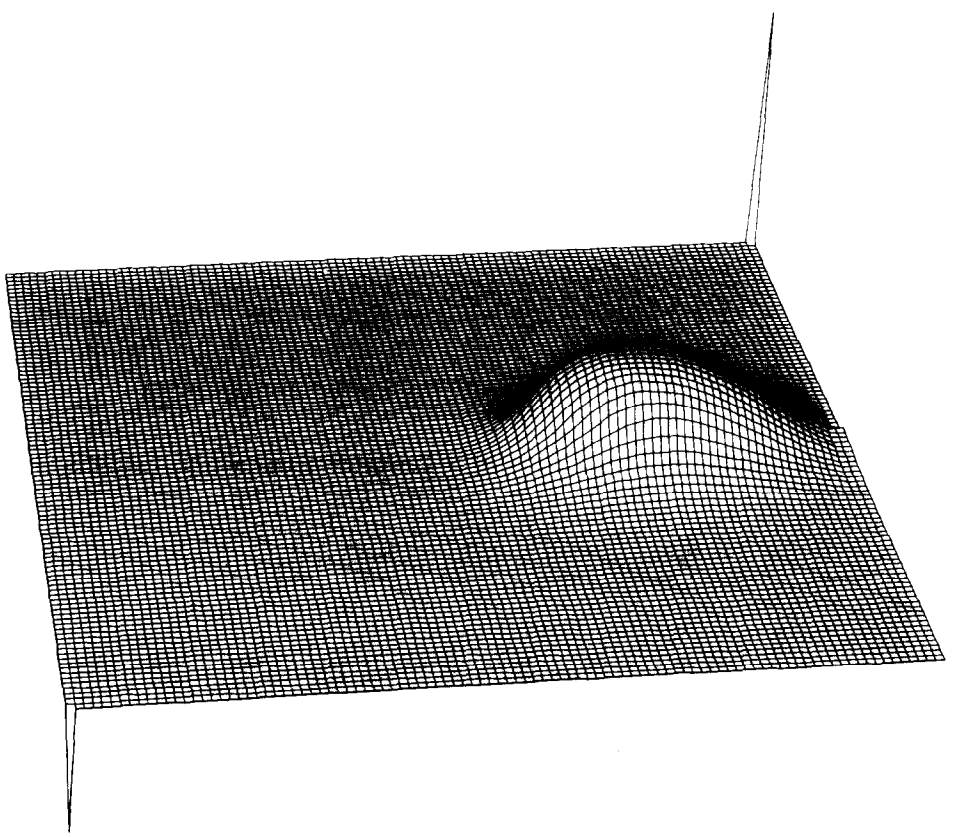

FIG. 12b. As in Fig. 12a but shown a quarter of a rotation earlier.

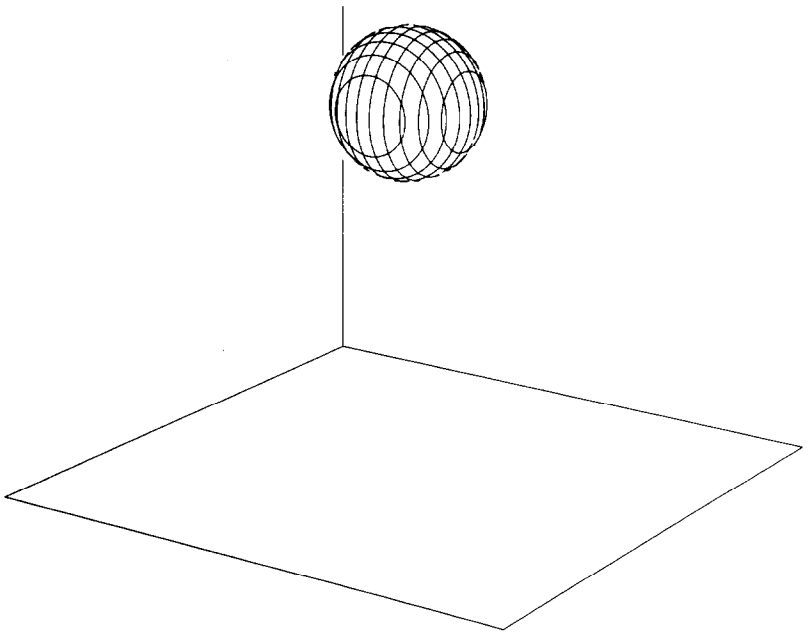

FIG. 13. Initial condition for the three-dimensional tests. All points in which the value of a function is greater than or equal to 0.5 are plotted.

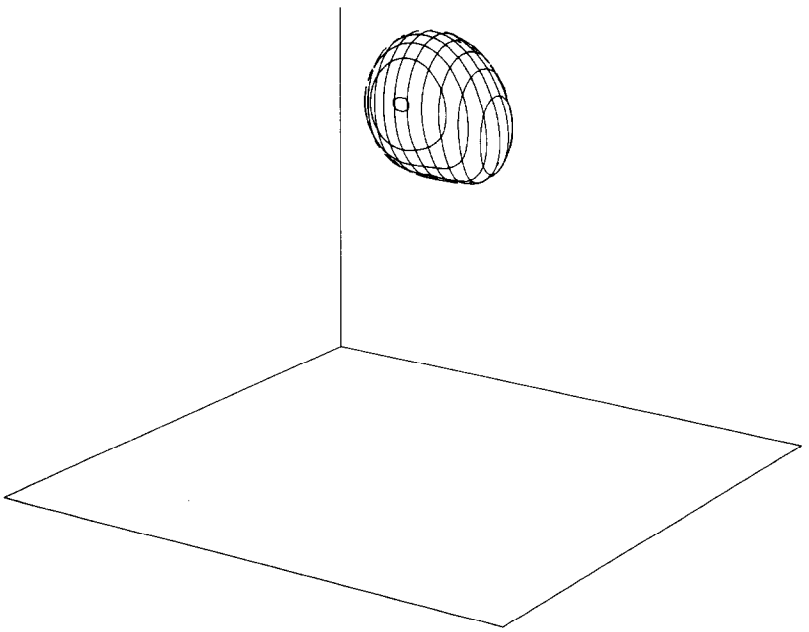

FIG. 14. Solution for the IORD = 4 scheme after five rotations. The values greater than or equal to 0.5 are plotted.

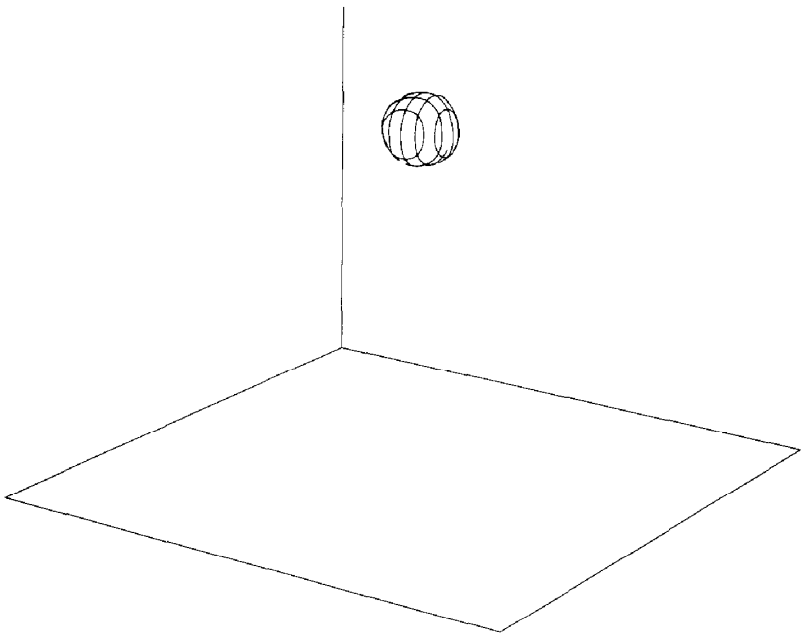

FIG. 15. As in Fig. 14 but the time-splitting version of the TVD scheme.

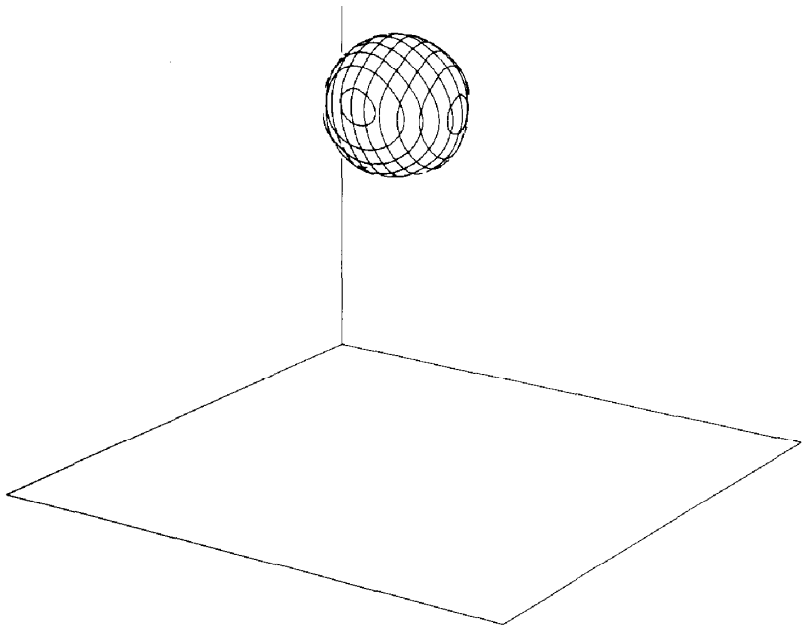

FIG. 16. As in Fig. 14 but for a modified, third-order-accurate in time version of the IORD = 4 scheme.

accurate in time (when the original velocity field is time independent) and third- or higher-order-accurate in space depending upon the number of iterations. The application of four iterations to the new version of the algorithm produces the results shown in Fig. 16 after five rotations. The maximum field value and ER2 are 2.69 and 0.54, respectively. It can be seen that the deformation that occurred with the basic version of scheme has almost totally vanished. Also, the implicit diffusion of the scheme is significantly decreased. On the other hand, the time-splitting form of the original scheme gives results similar to those shown in Fig. 14 (maximum value = 1.73, ER2 = 0.62). Finally, it can be concluded that including all third-order terms explicitly in the scheme is essential to eliminate the occurring deformation and improve the solution's accuracy. The results obtained suggest (there is not enough evidence to form a stronger conclusion) that isotropic distribution of the truncation error can be reached only for those advection schemes that are at least the same order of accuracy in both time and space as the dimensionality of the problem. The results obtained in [12] (the cross terms have been applied explicitly to different types of schemes) suggest that this formulated hypothesis is generally applicable.

5. Some Possible Options of the Scheme

In the previous sections the basic form of the algorithm has been presented and discussed in detail. The different assumptions on the truncation of the Taylor series expansion in the first step of the scheme development were shown to lead to the new versions of the algorithm. Using the same logical procedures as in the previous sections, one can construct many new schemes. Some of the existing options will be described below.

5.1. *Divergent Flow Field*

To obtain Eq. (7) a uniform velocity field had been assumed. When $u^I \equiv u^I(\mathbf{x})$, Eq. (7) takes the form

$$\left.\frac{\partial \psi}{\partial t}\right|_{\mathbf{i}}^{n} = \cdots - \sum_{I=1}^{M} \frac{\partial}{\partial x^I}\left[\left(0.5\,\Delta t\, u^I \sum_{J=1}^{M} \frac{\partial u^J}{\partial x^J}\right)\psi\right]\Bigg|_{\mathbf{i}}^{n} \tag{37}$$

where the terms that are not written explicitly are the same as in (7). Note that (37) proves that (7) and (13) are valid not only for a uniform velocity field but for any velocity field that is time independent and nondivergent. Using (37) results in a new, corrected form of (13):

$$\begin{aligned}\tilde{u}^I_{\mathbf{i}+(1/2)\mathbf{e}_I} = \cdots & -0.25\,\Delta t\, u^I_{\mathbf{i}+(1/2)\mathbf{e}_I}(u^I_{\mathbf{i}+(3/2)\mathbf{e}_I} - u^I_{\mathbf{i}-(1/2)\mathbf{e}_I})/\Delta X^I \\ & - 0.25\,\Delta t\, u^I_{\mathbf{i}+(1/2)\mathbf{e}_I} \sum_{\substack{J=1 \\ J\neq I}}^{M} (u^J_{\mathbf{i}+(1/2)\mathbf{e}_J} + u^J_{\mathbf{i}+(1/2)\mathbf{e}_J+\mathbf{e}_I} \\ & - u^J_{\mathbf{i}-(1/2)\mathbf{e}_J} - u^J_{\mathbf{i}-(1/2)\mathbf{e}_J+\mathbf{e}_I})/\Delta X^J \end{aligned} \tag{38}$$

where the terms omitted are the same as in (13). When the original velocity field is nondivergent the new terms in (38) are insignificant. They vanish in the second iteration of the scheme, while in higher iterations they are always an order smaller in ΔX than the original terms. It has been found that application of Eq. (38) to the tests presented in Section 4 practically does not affect the previously obtained results. On the other hand when the velocity is strongly convergent, application of Eq. (38) to the problem of the evolution of the droplet size distribution due to the evaporation–condensation process improves the results (William Hall, personal communication).

5.2. *Time-Dependent Velocity Field*

When the time dependence of the velocity field is taken into account, Eq. (7) should be written in the form

$$\left.\frac{\partial \psi}{\partial t}\right|_{\mathrm{i}}^{n} = \cdots + \sum_{l=1}^{M} \frac{\partial}{\partial x^l}\left(0.5\,\Delta t \frac{\partial u^l}{\partial t}\psi\right)\Bigg|_{\mathrm{i}}^{n} \tag{39}$$

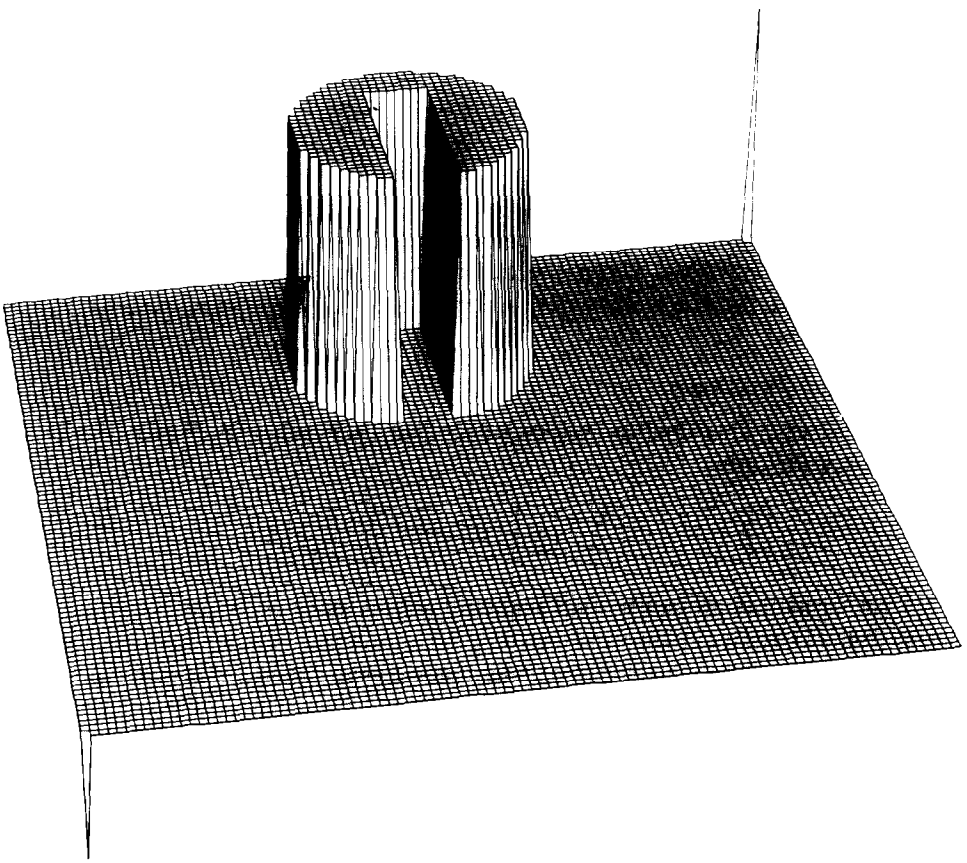

FIG. 17. Initial condition for the "shock-type initial condition problem" tests. Scale values in corners are the same as for Fig. 7.

where the terms not written explicitly are the same as in (7). The "antidiffusive" velocity (13) is written in the form

$$\tilde{u}^l_{i+(1/2)\mathbf{e}_l} = \cdots + 0.5\,\Delta t \frac{\partial u^l}{\partial t}\bigg|^n_{i+(1/2)\mathbf{e}_l} \tag{40}$$

where the omitted terms are the same as in (13). It is still unclear how to properly approximate the velocity time derivative in (40) in the case of a nonlinear equation such as the momentum equation. In applications in which time dependence of the velocity field is given a priori, Eq. (40) may be used in the second iteration of the scheme. Tests performed where the angular velocity from the previous section was allowed to be time dependent, $\omega \sim \cos(a \cdot t)$, suggest that the effect of Eq. (40) is negligible. This problem will be investigated more systematically in the future.

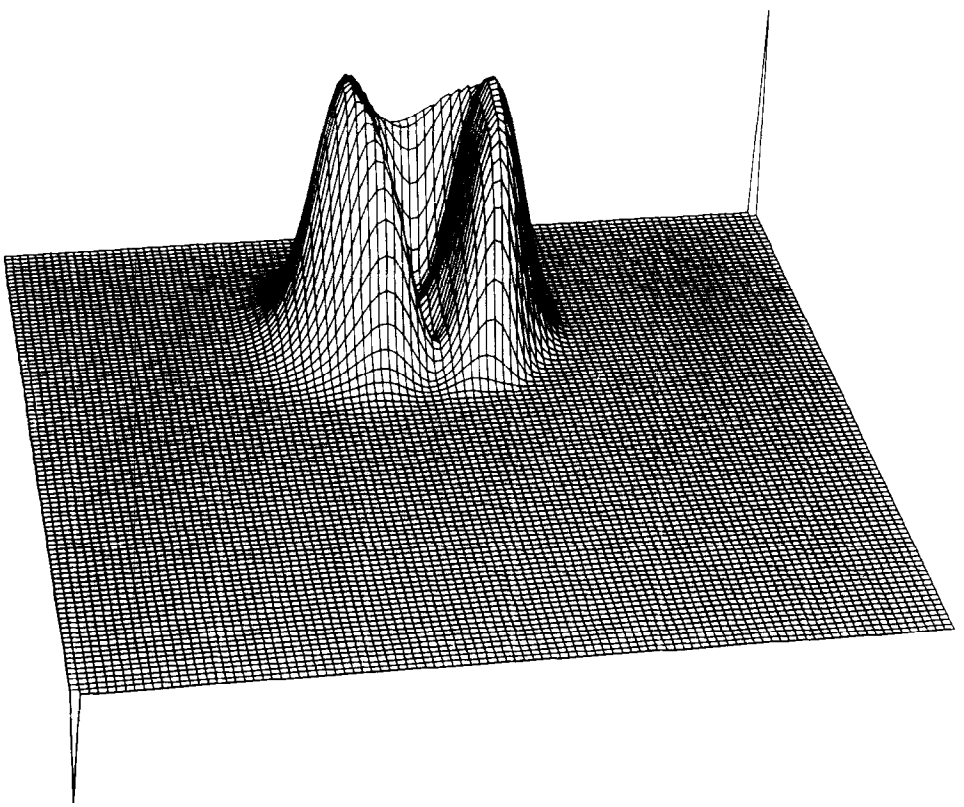

FIG. 18. Solution for the IORD = 4 scheme after one revolution.

5.3. *Schemes with a Higher Order of Accuracy in Time*

In Section 4 the development of the scheme that is third-order-accurate in time was presented. One can, similarly, construct schemes with an optional order of accuracy in time and space. Increasing the order of accuracy of the scheme results in additional terms in Eq. (7) and dramatically complicates the form of the "antidiffusive" velocity (13). It has been found that the application of the versions of the scheme that are third- and fourth-order-accurate in time, in both a time-splitting and a combined form, has little effect on the results of the two-dimensional tests from the previous section. It has been found that the third- or fourth-order accurate in time version of the scheme may have an important application to the "moving shock" problem.

5.4. *The Shock-Type Initial Condition Problem*

To illustrate the behavior of the scheme for a shock-type initial condition it is convenient to repeat the test proposed by Zalesak [14]. In the case of the two-

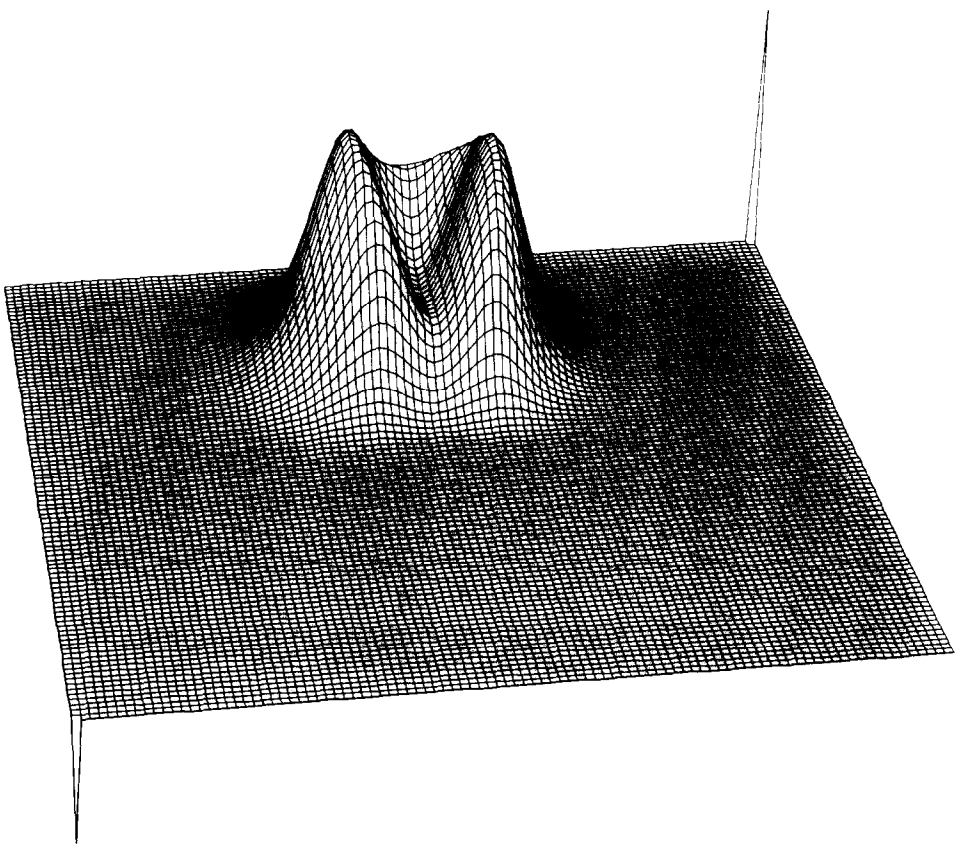

FIG. 19. As in Fig. 18 but for the IORD = 2 scheme.

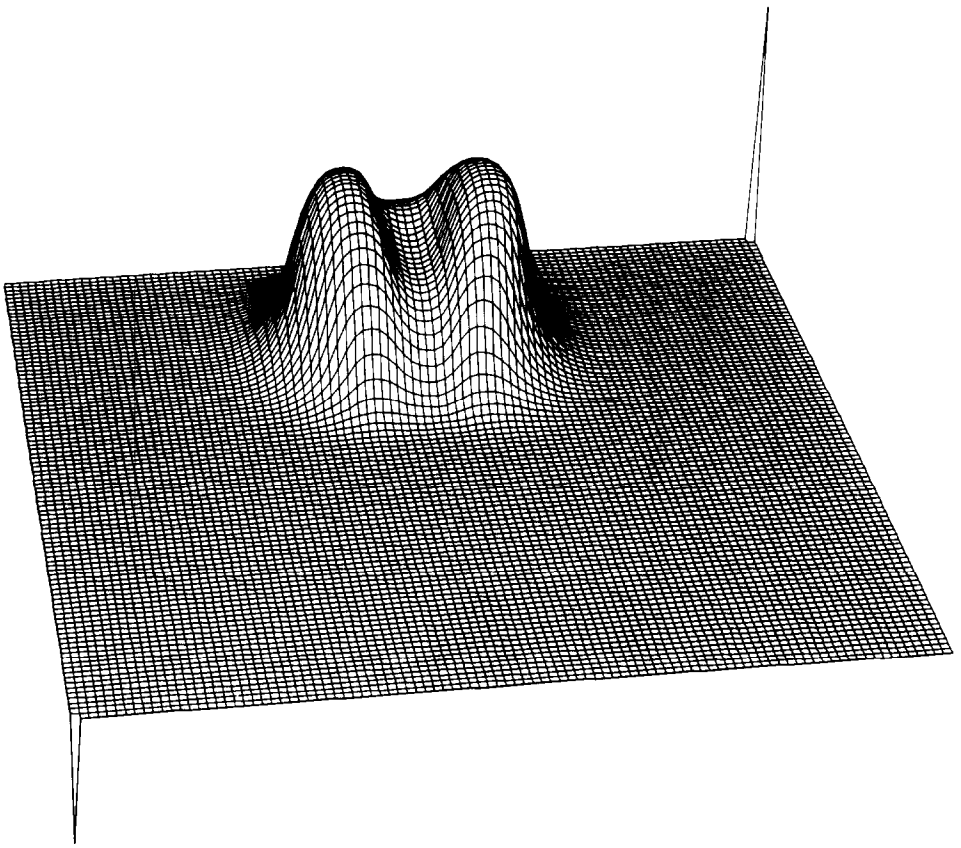

FIG. 20. As in Fig. 18 but for the TVD scheme.

dimensional test from the previous section the cone is replaced by a cylinder (with the same base radius, amplitude, and position as the cone) with a deep groove, as shown in Fig. 17. In Figs. 18, 19, and 20 the solutions after one revolution (as in [14]) are shown for IORD = 4, IORD = 2, and a combined TVD scheme. The maximum values and ER2 are, respectively, 4.76 and 0.28; 3.82 and 0.46; and 3.34 and 0.50. It can be seen that while the TVD scheme nearly maintains the flat shape of the cylinder's top, the proposed algorithm (especially for IORD = 4) creates an artificial maxima. This effect is an obvious consequence of the scheme structure and will always occur in the closest neighbourhood of the shock or contact discontinuity. In the category of problems in which this local amplification is unacceptable it is possible to eliminate this effect, for example, by turning off the corrective procedure in the closest neighbourhood of the shock. As an example, the semi-empirical "switch" is presented:

$$\mathrm{SW}^I_{\mathbf{i}+(1/2)\mathbf{e}_I} = \min(\lambda^I_{\mathbf{i}+(3/2)\mathbf{e}_I}, \lambda^I_{\mathbf{i}-(1/2)\mathbf{e}_I}) \tag{41a}$$

$$\lambda^I_{\mathbf{i}+(1/2)\mathbf{e}_I} = 0.5 \left\{ 1 + \mathrm{sign} \left[\left(\frac{|\psi^*_{\mathbf{i}} - \psi^*_{\mathbf{i}+\mathbf{e}_I}|}{\psi^*_{\mathbf{i}} + \psi^*_{\mathbf{i}+\mathbf{e}_I} + \varepsilon} - \mathrm{ES} \right) \frac{\psi^*_{\mathbf{i}} + \psi^*_{\mathbf{i}+\mathbf{e}_I}}{\psi^*_{\mathbf{i}} + \psi^*_{\mathbf{i}+\mathbf{e}_I} + \varepsilon} \right] \right\} \tag{41b}$$

where the constant ES was found experimentally to be $10^{-2} \geqslant \mathrm{ES} \geqslant 0.3 \cdot 10^{-2}$. The switch is constructed only after the first iteration of the scheme, and it remains constant in all consequent iterations. Note that SW is usually equal to unity and turns to zero when

$$\left. \frac{\partial \psi}{\partial x} \right|^n_{\mathbf{i}+(1/2)\mathbf{e}_I} = 0$$

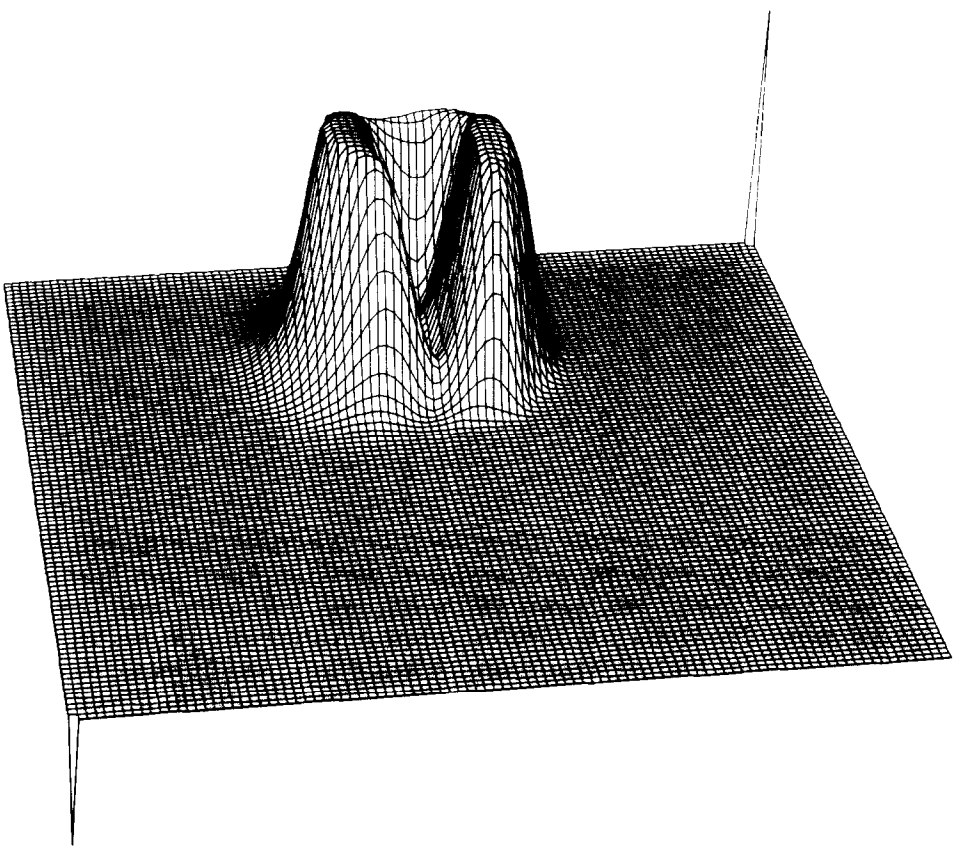

FIG. 21. As in Fig. 18 but for the time-splitting version of the IORD = 4 scheme with the switch (41) applied.

and $\bar{\psi}_{i+(1/2)e_l} \neq 0$. Modified "antidiffusive" velocity takes the form

$$u^{l,(\sim)k}_{i+(1/2)e_l} = (u^{l,(\sim)k}_{i+(1/2)e_l})_{\text{Eq.(13)}} \times \text{SW}^l_{i+(1/2)e_l}, \qquad k = 1,..., \text{IORD} - 1. \tag{42}$$

The optimal value of the constant ES in (41b) was found to be 0.3×10^{-2} for all cases tested. Larger values of the ES produce more diffusive solutions, while smaller ones do not eliminate the amplification effect totally. The solutions for the IORD = 4 scheme applied in a time-splitting and a combined form are shown in Figs. 21 and 22, respectively. The slight difference between these two solutions is caused by the switch rather than the scheme itself. The switch should not be universally applied because it affects the solutions for non-shock-type initial conditions. In Fig. 23 the solution after six rotations of the cone is shown for the IORD = 4 scheme with the switch (41a, b) applied. The solution obtained is less diffusive than for the TVD scheme

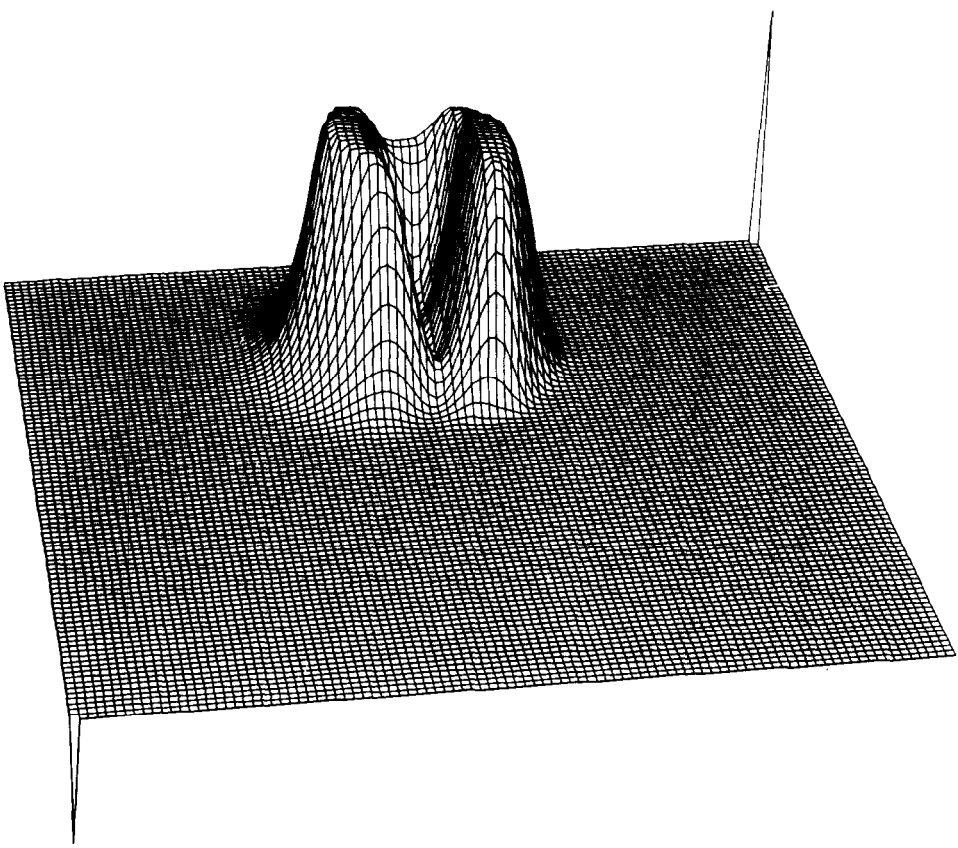

FIG. 22. As in Fig. 21 but for the combined scheme.

(Figs. 12a, b) but significantly more diffusive than for the original IORD = 4 scheme (Fig. 10). The universal character of the constant ES is still unknown and in this point the switch presented needs to be improved. In its current form it should be interpreted only as an example indicating one of the possibilities of the shock problem solution.

In the special case of a shock occurring on the "lee" side of the initial condition, a monotonicity-preserving solution is provided by the third-order-accurate in time version of the algorithm (36). In Figs. 24a and 24b the results of the one-dimensional tests ($u = \Delta X = 1$, $\Delta t = 0.5$) are shown, respectively, for the basic (13) and modified (36) versions of the scheme. For comparison, the solutions for the TVD scheme are also plotted (dashed lines). It can be seen that application of the "antidiffusive" velocities given by Eq. (36) totally eliminates the amplification effect produced by the basic version of the algorithm. The solution obtained is less diffusive than the one

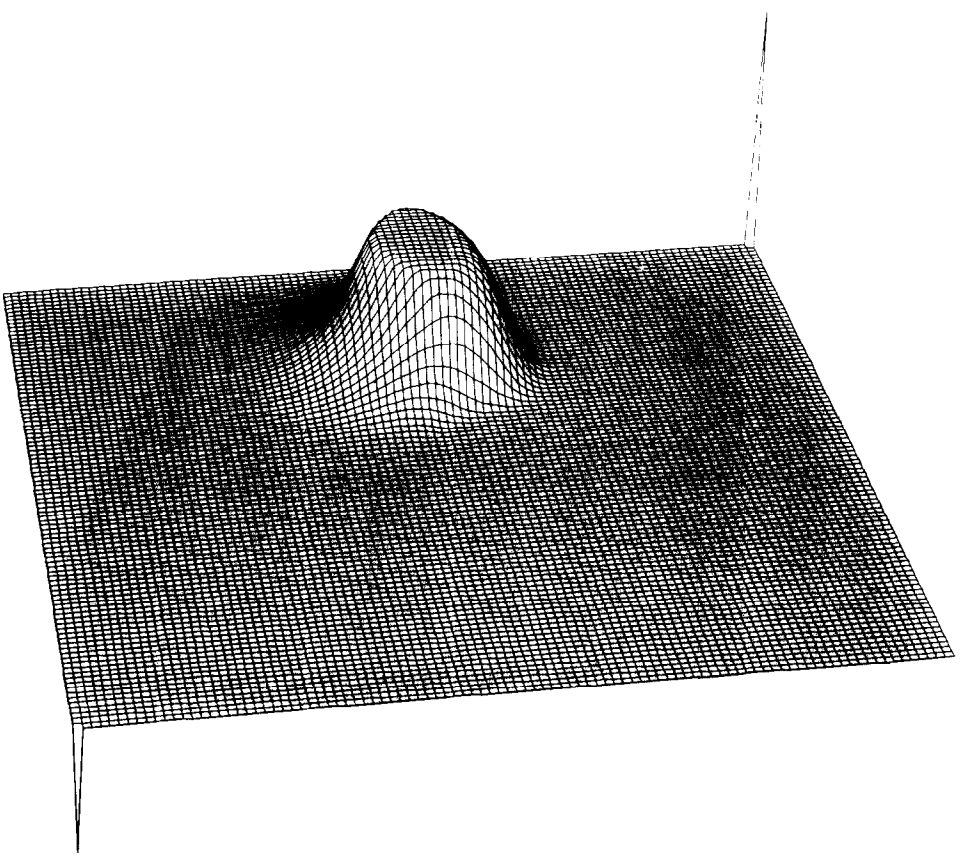

FIG. 23. Solution after six rotations for the scheme shown in Fig. 22 but applied to the initial condition in Fig. 7.

produced by the TVD scheme. On the other hand, when the shock occurs on the "wind" side of the initial condition, the amplification effect produced by the basic version of the scheme (Fig. 25a) transforms to oscillations for the modified version of the algorithm (Fig. 25b). This result suggests a different construction of the switch than previously discussed. For example, if in the first term of the one-dimensional version of Eq. (36) $u(\Delta X)^2$ is replaced by the sign $(\psi_i^* - \psi_{i+1}^*)\,|u|\,(\Delta X)^2$, the result will be a scheme with properties similar to those of the tested version of the TVD scheme.

5.5. *Practical Simplification of the Scheme*

In cases when computational efficiency is essential for a problem one may find the IORD = 2 scheme is the only practical one to apply. Although this simplest version of the algorithm produces results of the quality comparable with that of the TVD scheme, it is significantly less accurate than the versions with IORD > 2. In [13] a simple compromise between accuracy and computational efficiency was presented.

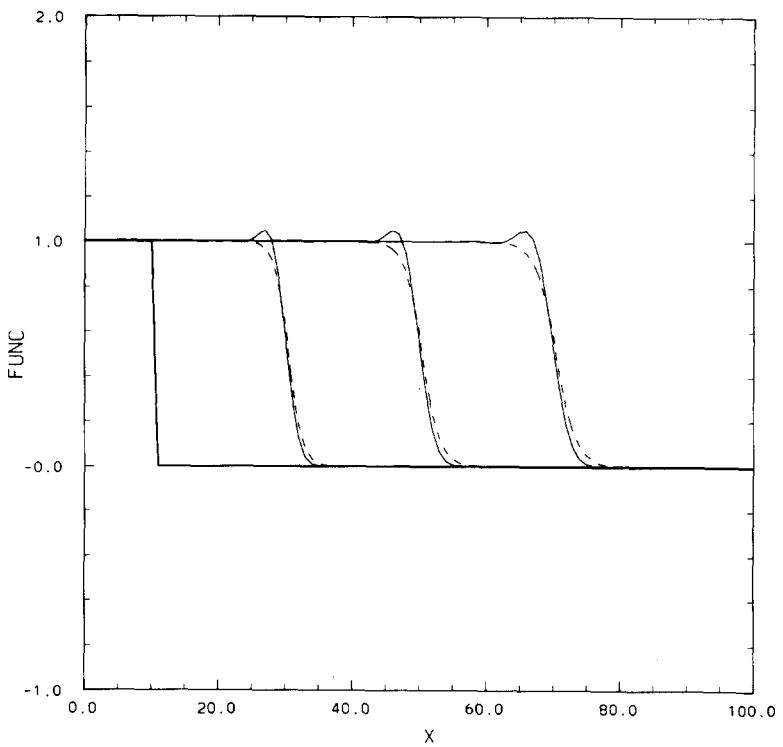

FIG. 24a. Different stages of the shock (heavy solid line) propagation (40, 80, 120 time steps). Solid lines: IORD = 4 scheme; dashed lines: TVD scheme.

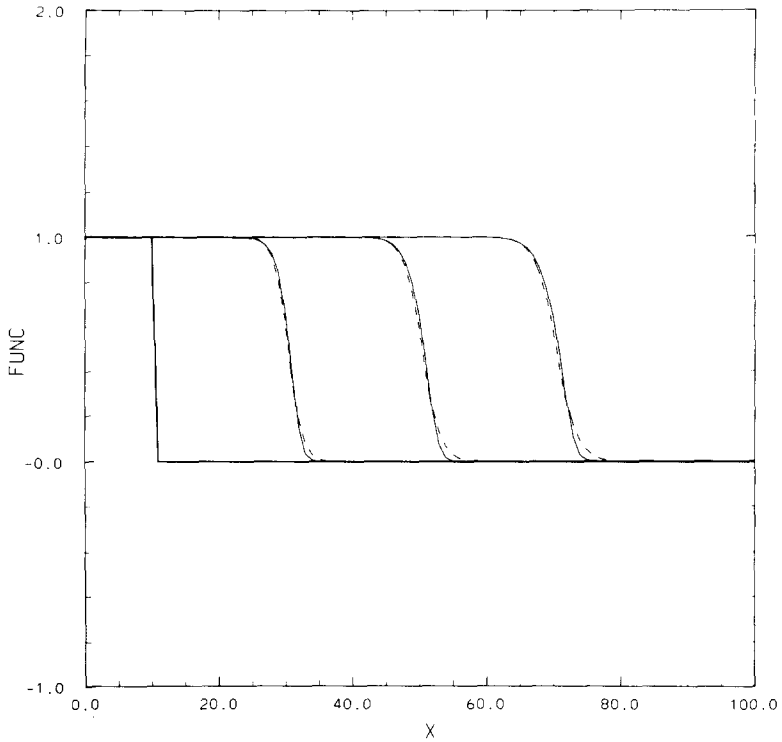

FIG. 24b. As in Fig. 24a but for IORD = 4 third-order-accurate in time scheme.

Because usually the antidiffusive velocities are smaller than the ones allowed by the stability criteria, it is possible to increase them by multiplying by some factor Sc.

$$\tilde{u}^l_{i+1/2} = (\tilde{u}^l_{i+(1/2)\mathbf{e}_l})_{\text{Eq. (13)}} \times \text{Sc}. \tag{43}$$

It was found experimentally that even a small increase of Sc over unity (e.g., Sc = 1.06) significantly improves the solution for the IORD = 2 scheme. In Fig. 26 the solution of the two-dimensional test from Section 4 is shown after six rotations for the IORD = 2 scheme with Eq. (43) applied and Sc = 1.06 (cf. Fig. 8). The maximum solution value and ER2 are, respectively, 3.17 and 0.31. It was found that the optimal value of the coefficient Sc depends upon the CFL number and dimensionality of the problem. The character of this dependence is still unknown. In some problems it may be worthwhile to tune Sc using some simple tests.

The scheme can also be simplified in a different way. In the presented basic version of the algorithm the general form of the "antidiffusive" velocity is $\tilde{u} = \tilde{u}(\psi^*, u)$. It was found that the form $\tilde{u} = \tilde{u}(\psi, u)$ can be used as well. This new form of the

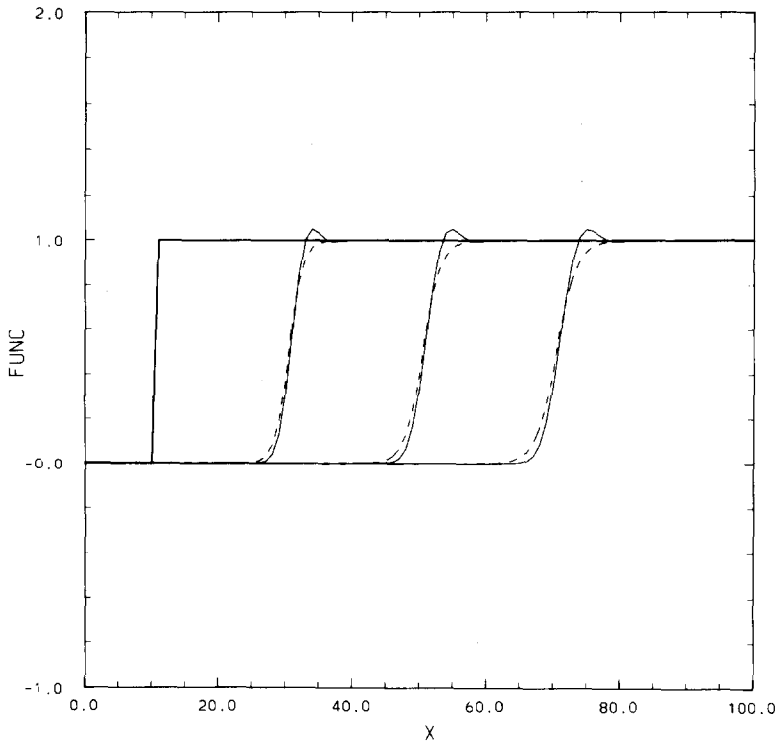

FIG. 25a. As in Fig. 24a but for a shock occurring on the "wind" side of the initial condition.

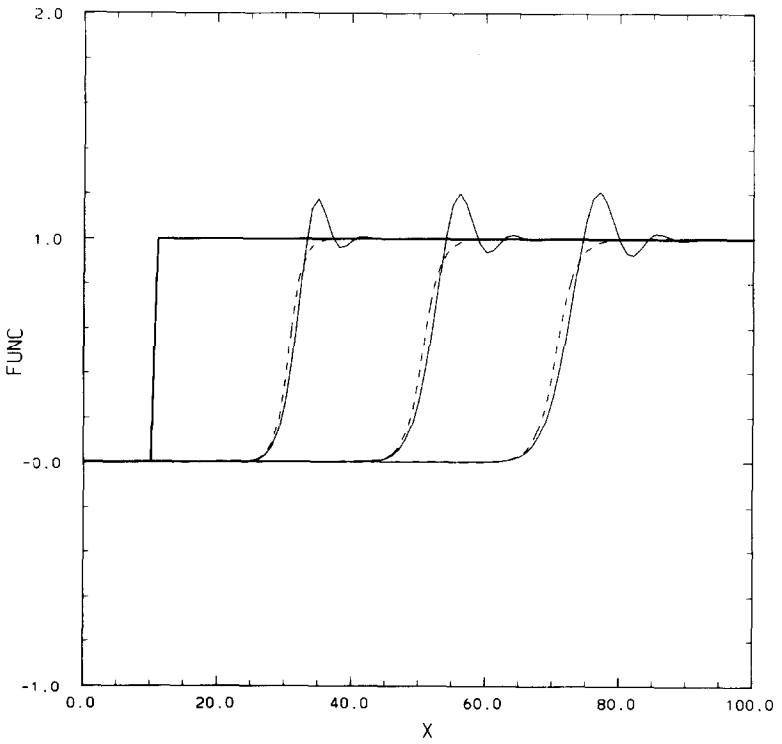

FIG. 25b. As in Fig. 24b but for an initial condition as in Fig. 25a.

"antidiffusive" velocity results in slightly larger truncation errors but gives final results close to those produced by the original algorithm. Using this information, the "antidiffusive" velocity for the IORD = 2 scheme may be modified, that is,

$$\tilde{u}_{\text{modified}} = \tilde{u} + \tilde{u}(\tilde{u}, \psi^*) \tag{44a}$$

or

$$\tilde{u}_{\text{modified}} = \tilde{u} + \tilde{u}(\tilde{u}, \psi). \tag{44b}$$

In Fig. 27 the solution of the cone rotation test after six revolutions is shown for the IORD = 2 scheme with (44a) applied. The maximum solution value and ER2 are 3.02 and 0.23, respectively (cf. Figs. 8 and 26). The disadvantage of this method is a more restrictive stability criterion of $\mathscr{C} \leqslant 0.5$ in (4).

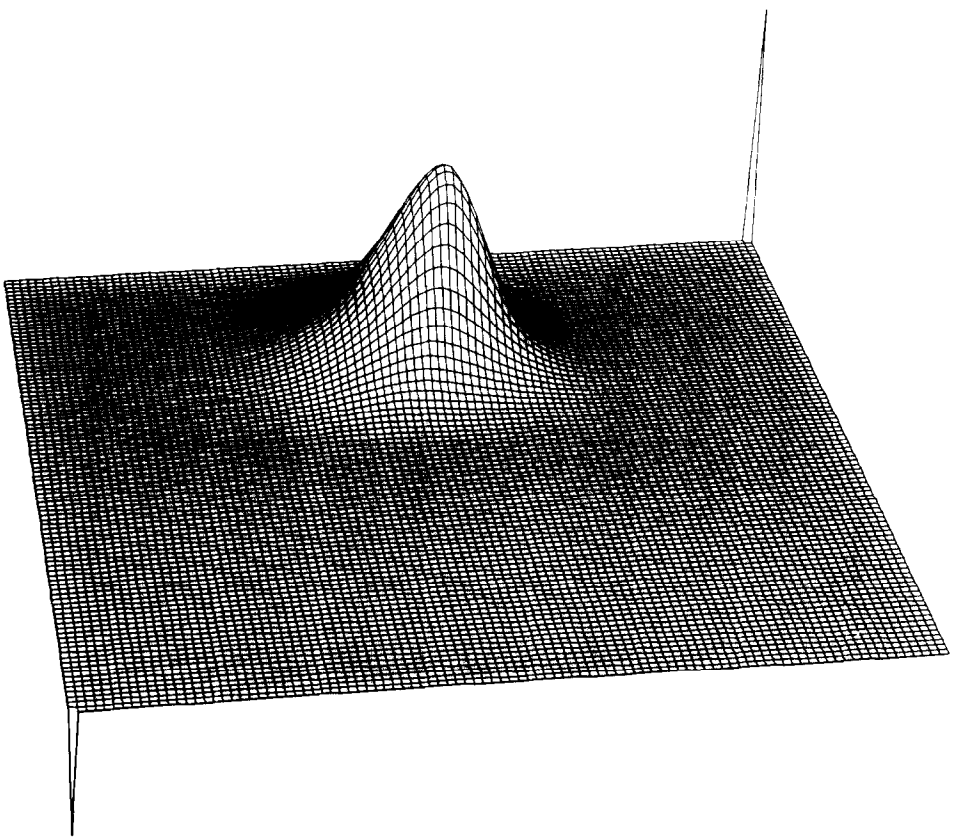

FIG. 26. As in Fig. 8 but with Sc = 1.06 in Eq. (43) applied.

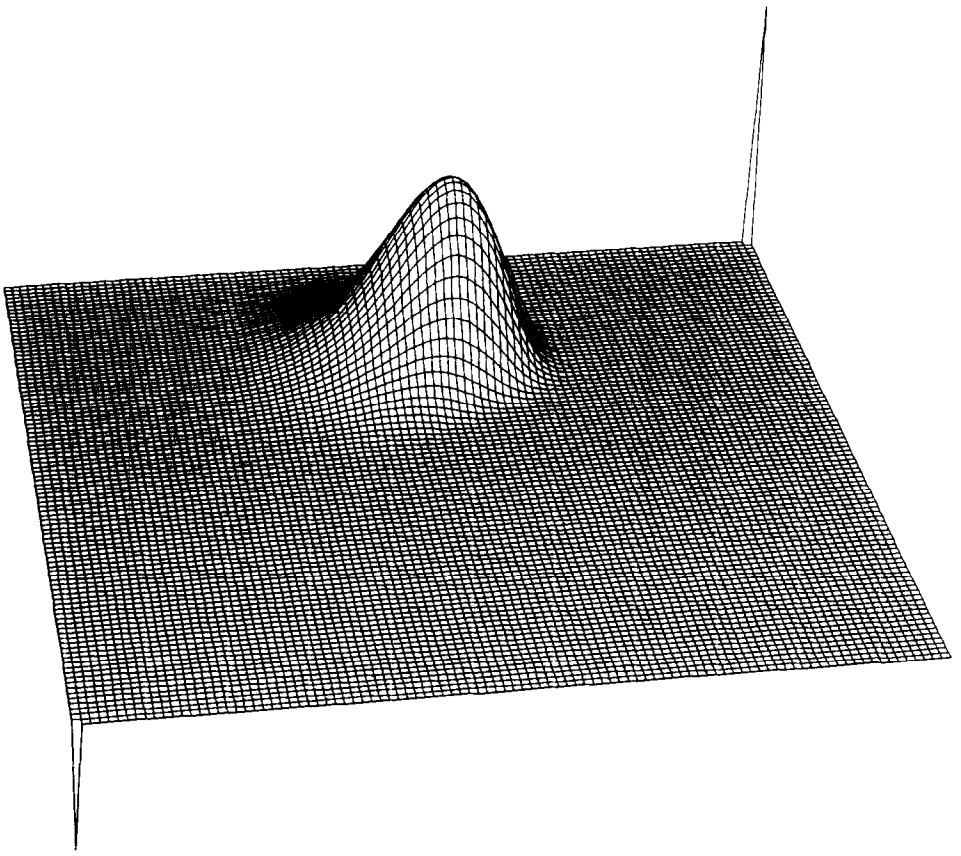

FIG. 27. As in Fig. 8 but with Eq. (44a) applied.

6. CONCLUSIONS

1. Using an iterative approach based upon the "upstream" scheme, a class of fully multidimensional, nonlinear, computationally efficient positive definite advective transport algorithms has been constructed. The simplest version of the developed schemes is second-order-accurate in both time and space. The most accurate version tested in this paper is third-order-accurate in time and fifth-order-accurate in space. In principle it is possible to construct an algorithm with an optional order of accuracy in time and space.

2. Results presented in this paper suggest that there exists a general connection between the distribution of the truncation error of any advection scheme and the dimensionality of the problem. It is suggested that to ensure that the numerical

solution of the advection equation be free of strong artificial deformations it is necessary to use schemes of at least the same order of accuracy in both time and space as the dimensionality of the problem.

3. The procedures were discussed whereby the basic form of the algorithm can be modified, depending on the user's requirements. Among others, such options as a generalization of the scheme for a divergent flow field case or the construction of a monotonicity-preserving scheme have been mentioned.

ACKNOWLEDGMENTS

The author is grateful to Dr. Terry L. Clark of NCAR for his suport in this project as well as for his helpful discussion and criticism of the manuscript. The author also wishes to thank Dr. William D. Hall for his criticism of the manuscript and Mary Davis for typing the manuscript. I wish to acknowledge the support received from the Advanced Study Program of NCAR while doing this research.

REFERENCES

1. D. L. BOOK, J. P. BORIS, AND K. HAIN, *J. Comput. Phys.* **18** (1975), 248.
2. J. P. BORIS AND D. L. BOOK, *J. Comput. Phys.* **11** (1973), 38.
3. J. P. BORIS AND D. L. BOOK, *J. Comput. Phys.* **20** (1976), 397.
4. T. L. CLARK, *J. Atmospheric Sci.* **36** (1979), 2191.
5. T. L. CLARK AND W. D. HALL, *J. Atmospheric Sci.* **36** (1979), 470.
6. A. HARTEN, *Math. Comp.* **32** (1978), 363.
7. A. HARTEN, "High Resolution Scheme for Hyperbolic Conservation Laws," New York Univ. Report, DOE/ER/03077-167, March 1982.
8. A. HARTEN, "On a Class of High Resolution Total-Variation-Stable Finite-Difference Schemes," New York Univ. Report, DOE/ER/03077-176, October 1982.
9. A. HARTEN AND G. ZWAS, *J. Comput. Phys.* **9** (1972), 568.
10. R. D. RICHTMYER AND K. W. MORTON, "Difference Methods for Initial-Value Problems," p. 405, Interscience–Wiley, New York, 1967.
11. P. J. ROACHE, "Computational Fluid Dynamics," p. 446, Hermosa Publ., Albuquerque, 1976.
12. P. K. SMOLARKIEWICZ, *Monthly Weather Rev.* **110** (1982), 1968.
13. P. K. SMOLARKIEWICZ, *Monthly Weather Rev.* **111** (1983), 479.
14. S. T. ZALESAK, *J. Comput. Phys.* **31** (1979), 335.